NASA TECHNICAL NOTE

NASA TN D-3676

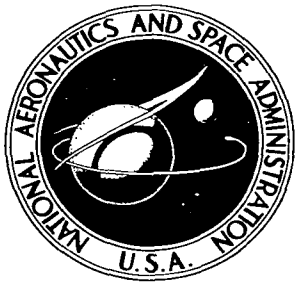

NASA TN D-3676

EXPLORATORY FLIGHT INVESTIGATION AND ANALYSIS OF STRUCTURAL LOADS ENCOUNTERED BY A HELICOPTER HINGELESS ROTOR SYSTEM

by John F. Ward

Langley Research Center

Langley Station, Hampton, Va.

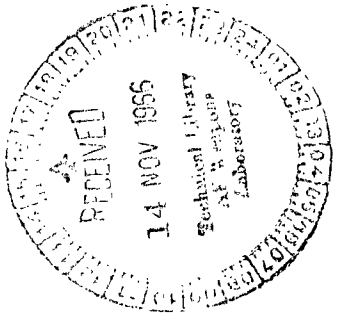

NATIONAL AERONAUTICS AND SPACE ADMINISTRATION • WASHINGTON, D. C. • NOVEMBER 1966

EXPLORATORY FLIGHT INVESTIGATION AND ANALYSIS OF STRUCTURAL LOADS ENCOUNTERED BY A HELICOPTER HINGELESS ROTOR SYSTEM

By John F. Ward

Langley Research Center
Langley Station, Hampton, Va.

NATIONAL AERONAUTICS AND SPACE ADMINISTRATION

For sale by the Clearinghouse for Federal Scientific and Technical Information
Springfield, Virginia 22151 – Price $2.00

EXPLORATORY FLIGHT INVESTIGATION AND ANALYSIS OF STRUCTURAL LOADS ENCOUNTERED BY A HELICOPTER HINGELESS ROTOR SYSTEM

By John F. Ward
Langley Research Center

SUMMARY

This paper presents the results of an exploratory flight research program and analytical investigation of the structural load characteristics of the helicopter hingeless rotor system. The rotor used in the flight program was an experimental three-blade hingeless rotor on an OH-13G helicopter. The basic dynamic response characteristics of the hingeless rotor system are reviewed to provide a background for the discussion and analysis of the structural loadings encountered in flight.

The results of the investigation indicate that at normal rotor rotational speed the centrifugal-force field provides approximately 95 percent of the cantilever-blade stiffening in the flapwise degree of freedom. Thus, the cantilever blade deflects in the first flapwise mode an amount virtually equal to a hinged blade and simultaneously provides rotor-hub moments which are an order of magnitude greater than those obtainable from a typical hinged rotor system. The investigation demonstrated that the structural load of most concern, for a hingeless rotor utilizing blades of conventional design, is the buildup of the blade cyclic chordwise bending moment in maneuvering flight throughout the speed range.

A simplified analysis of the hingeless-rotor blade root bending moments is developed and compared with measured data. This analysis makes use of the virtual offset untwisted blade with spring restraint to approximate the response of the actual cantilever blade. Only the aerodynamic effects of twist are included in the analysis. The results indicate that, for preliminary studies, a conventional offset blade analysis can be utilized provided that the proper virtual spring restraint is used at the flapping and lagging hinges.

INTRODUCTION

The renewed interest in the helicopter hingeless rotor system stems from the fact that a number of significant benefits can be realized with the successful utilization of such

a rotor system. The essential feature of the hingeless rotor system is the removal of the conventional articulated rotor flapping and lagging hinges and cantilevering the rotor blades directly from the rotor drive shaft. Because of the cantilever action of the blades, large rotor-hub moments can be developed and transferred directly from the rotor into the fuselage as a strong source of aircraft pitching and rolling control moment and damping moment. This can result in an order of magnitude improvement in the helicopter control power and damping capability, which leads to significant, and much needed, improvements in the handling qualities of the helicopter. The elimination of the hinges and associated hardware also provides an opportunity for a substantial reduction in rotor-hub complexity, mechanical maintenance, and rotor-hub aerodynamic drag.

The cantilever rotor design is not new to the helicopter field. During the initial development of the helicopter and autogyro, cantilever blade systems were tried but were abandoned because of problems with rotor control and high blade stresses. These problems were solved by introducing blade articulation and subsequent helicopter development concentrated on the refinement of the hinged-rotor system. Occasional unsuccessful attempts have been made in the past to develop a "rigid" rotor system. The current designs, in contrast to early rigid rotors, do not attempt to eliminate flexibility in the rotor system. As pointed out in reference 1, it is believed that most, if not all, of the early failures with rigid rotors involved deliberate attempts at preventing rotor system flexibility. Current hingeless-rotor designs (refs. 2 and 3) do not attempt to avoid flexibility but varying amounts are used in an effort to control the rotor dynamic response, blade cyclic stress levels, and helicopter vibration levels.

In principle, the hingeless rotor system represents a basic departure from the articulated-rotor-system concept for which there exists a considerable background of research and design information. In order to make an initial assessment of the aeroelastic characteristics of the hingeless system and to begin accumulating research information a flight research program was undertaken by the National Aeronautics and Space Administration. The results of the experimental and analytical structural loads investigation carried out in this program are summarized in this paper. The results of a flying-qualities investigation, which was conducted as part of the overall flight program, are presented in reference 4.

A review of the general dynamic response characteristics of a hingeless rotor is presented as background prior to discussing the results of the structural loads investigation. The analytical treatment utilizes the concept of a virtual offset hinge blade with spring restraint at the hinge to simulate the hingeless-blade first-bending-mode response. The analytical work modifies the material presented in reference 5 and extends the equivalent offset approach to include the blade lagging degree of freedom. This modified approach allows the calculation of critical blade bending moments with the use of

conventional offset hinge rotor aerodynamics together with conventional equations of motion suitably modified for the inclusion of the hinge spring restraint. A comparison of the results of this simplified approach with the experimental results provides an indication of what success might be expected when utilizing the approximate analysis in preliminary design, where a detailed and rigorous aeroelastic analysis might not be warranted.

SYMBOLS

A_1 lateral cyclic pitch angle or coefficient of $-\cos\psi$ in expression for Θ, positive for nose up at $\psi = 180^o$, radians

a section lift-curve slope

a_o blade mean flapping angle relative to plane perpendicular to rotor shaft, positive for displacement in direction of positive thrust, radians

a_1 coefficient of $-\cos\psi$ in expression for β_1, positive for upward flapping relative to plane perpendicular to rotor shaft at $\psi = 180^o$, radians

B blade tip loss factor

B_1 longitudinal cyclic pitch angle or coefficient of $-\sin\psi$ in expression for Θ, positive for nose up at $\psi = 270^o$, radians

b_1 coefficient of $-\sin\psi$ in expression for β_1, positive for upward flapping relative to plane perpendicular to rotor shaft at $\psi = 270^o$, radians

C_T rotor thrust coefficient, $\frac{\text{Rotor thrust}}{\pi R^2 \rho (\Omega R)^2}$

c blade chord, feet (meters)

c_l blade section lift coefficient

D drag on blade element, pounds (newtons)

e_v offset of virtual hinge from center line of rotor shaft, feet (meters)

g gravitational acceleration, feet per second^2 (meters per second^2)

I_V mass moment of inertia of blade about virtual hinge, slug-feet^2 (kilogram-meter^2)

K_{VF} spring constant of blade virtual flapping hinge spring, foot-pounds per radian (meter-newtons per radian)

K_{VL} spring constant of blade virtual lagging hinge spring, foot-pounds per radian (meter-newtons per radian)

K_{1F} blade first-mode flapping Southwell coefficient, $\frac{\omega_{1R}^2 - \omega_{1NR}^2}{\Omega^2}$

K_{1L} blade first-mode lagging Southwell coefficient, $\frac{\nu_{1R}^2 - \nu_{1NR}^2}{\Omega^2}$

L lift on blade element, pounds (newtons)

M_H total rotor-hub moment, foot-pounds (meter-newtons)

$M_{H,A}$ longitudinal component of rotor-hub moment, positive for nose-up moment applied to aircraft, foot-pounds (meter-newtons)

$M_{H,B}$ lateral component of rotor-hub moment, positive for right rolling moment applied to aircraft foot-pounds (meter-newtons)

M_{VF} moment about virtual flapping hinge, foot-pounds (meter-newtons)

M_{VL} moment about virtual lagging hinge, foot-pounds (meter-newtons)

M_W blade weight moment about virtual flapping hinge, inch-pounds (meter-newtons)

$M_{c,1}$ first-harmonic cantilever-blade chordwise structural bending moment, positive for moment opposite to rotor rotation, inch-pounds (meter-newtons)

m mass of blade per foot of radius, slugs per foot (kilograms per meter)

n number of blades

p helicopter rolling velocity, positive for right roll, radians per second

q	helicopter pitching velocity, positive for nose-up pitching, radians per second
R	blade radius, feet (meters)
r	distance measured along blade from axis of rotation to blade element, feet (meters)
S_{VF}	shear force at virtual flapping hinge, positive upward in plane of flapping, pounds (newtons)
T	thrust on blade element, pounds (newtons)
t	time, seconds
U	resultant velocity perpendicular to blade-span axis at blade element, feet per second (meters per second)
$U_{P,S}$	component at blade element of resultant velocity perpendicular both to blade-span axis and $U_{T,S}$, feet per second (meters per second)
$U_{T,S}$	component at blade element of resultant velocity perpendicular to blade-span axis and to shaft axis, feet per second (meters per second)
V	velocity along flight path, knots
v	induced inflow velocity at rotor, positive downward, feet per second (meters per second)
W	weight of blade outboard of virtual hinge, pounds (newtons)
w_1	blade first-flapwise-mode shape
w_{1R}	rotating blade first-flapwise-mode shape
x	ratio of blade-element radius to rotor-blade radius, r/R
α	blade-element angle of attack, measured from line of zero lift, radians
β_1	blade first-harmonic flapping angle with respect to plane perpendicular to axis of rotor shaft, $-a_1 \cos \psi - b_1 \sin \psi$, radians

Γ_F blade flapping response coefficient

Γ_L blade lagging response coefficient

$\Gamma_{\beta,1}$ blade flapwise response amplification factor (see eq. (A4))

γ mass constant of uniform cantilever blade, $\frac{\rho acR^4}{\frac{1}{3}mR^3}$

γ_v blade mass factor (Lock number) based on virtual hinge offset, $\frac{\rho acR^4}{I_v}$

δ_1 aerodynamic damping coefficient in first flapwise bending mode (see eq. (A5))

ζ_1 first-harmonic blade lagging motion displacement in a plane perpendicular to the rotor shaft, positive in direction opposite to rotor rotation, radians

η aircraft normal load factor

Θ instantaneous blade-section pitch angle, angle between line of zero lift of blade section and plane perpendicular to rotor shaft, $\theta_o + \theta_t x + \theta_1$

θ_o collective pitch angle at blade root, average value of instantaneous blade-root pitch angle around azimuth, radians

θ_t difference between root and tip pitch angles, positive when tip angle is larger, radians

θ_1 first-harmonic cyclic pitch angle, $-A_1 \cos \psi - B_1 \sin \psi$, radians

λ_s inflow ratio, $-v/\Omega R$ for hover

ν_{1NR} blade first-chordwise-mode natural frequency, nonrotating, radians per second

ν_{1R} blade first-chordwise-mode natural frequency, rotating, radians per second

ξ_v nondimensional offset of virtual hinge, e_v/R

ρ mass density of air, slugs per foot^3 (kilogram per meter^3)

σ_v blade first mass moment about virtual hinge, slug-feet (kilogram-meters)

τ resultant aircraft angular velocity, $(q2 + p2)^{1/2}$

$\Phi_{\beta,1}$ phase lag of blade first-mode flapping response to cyclic control input (see eq. (A6))

ϕ inflow angle at blade element in plane perpendicular to blade-span axis, $\tan^{-1} \frac{U_{P,s}}{U_{T,s}}$, radians

ψ blade azimuth angle measured from downwind position in direction of rotor rotation, radians

$\psi_{c,1}$ azimuth angle of positive peak of the blade first-harmonic chordwise bending-moment oscillation, radians

$\psi_{\beta,1}$ azimuth angle of positive peak of the blade first-harmonic flapwise bending-moment oscillation, radians

$\psi_{\theta,1}$ azimuth angle of positive peak of the blade first-harmonic cyclic feathering-motion oscillation, radians

ψ_τ azimuth angle of resultant aircraft angular velocity, $\tan^{-1} \frac{-p}{-q}$, radians

Ω rotor rotational speed about shaft axis, radians per second

Ω_n normal operation rotor rotational speed, radians per second

ω_{1NR} blade first-flapwise-mode natural frequency, nonrotating, radians per second

ω_{1R} blade first-flapwise-mode natural frequency, rotating, radians per second

$| \; |$ absolute magnitude

Dots over symbols denote derivatives with respect to time t; bars over symbols denote derivatives with respect to azimuth angle ψ.

GENERAL CHARACTERISTICS OF HINGELESS ROTOR

The hingeless rotor is sometimes referred to as a rigid rotor system. Although this terminology focuses attention on the primary difference between hingeless and articulated rotors, it must be recognized that the use of flexibility is the key to the successful utilization of the hingeless-rotor concept. From the standpoint of blade dynamics, the hingeless rotor represents a fundamental change from dealing with the articulated-blade dynamic response in the rigid-body pendulum mode to dealing with the cantilever-blade dynamic response in the first-bending mode. Certainly a rigorous treatment of either configuration would deal with higher order bending modes but it is the nature of the first-mode response characteristics that determines the fundamental differences in the two rotor systems.

In the analysis of hingeless-rotor dynamics and structural loads both the blade flapwise and chordwise degrees of freedom are of concern. The following section deals with the similarity between hinged- and cantilever-blade flapping response. The blade chordwise (or lagging) degree of freedom is treated in later sections dealing with equivalent blade systems and blade chordwise bending moments.

Blade Flapping Response

A comparison of the conventional hinged blade and the hingeless, or cantilever, blade first-mode natural frequencies as a function of rotor speed is shown in figure 1.

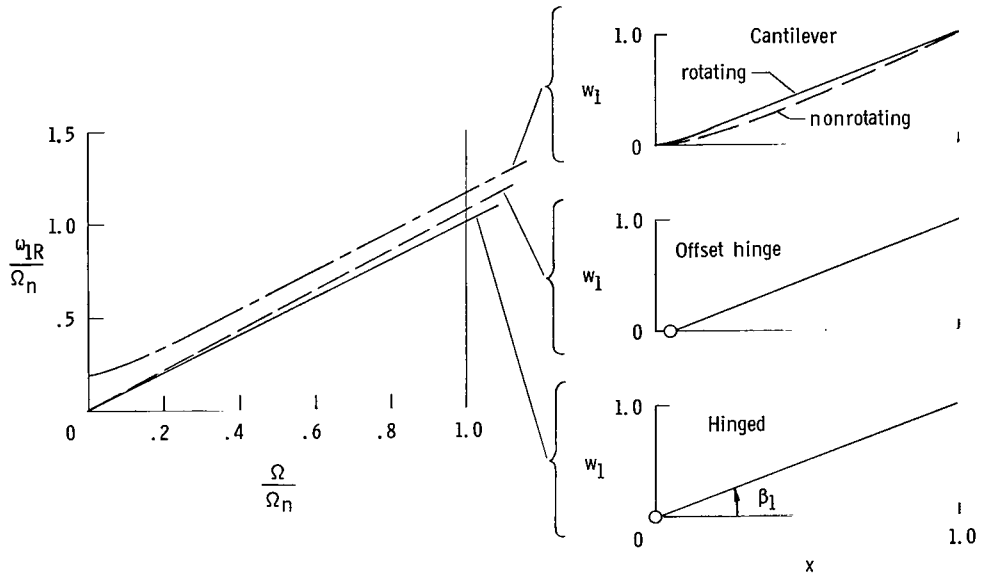

Figure 1.- Rotor-blade natural frequencies and mode shapes.

This comparison utilizes frequencies and mode shapes for untwisted blades. A curve of the first-mode natural frequency in the flapwise degree of freedom, as a function of rotor rotational speed, is given for each of three uniform blade configurations: (1) zero-offset hinged blade, (2) conventional offset hinged blade, and (3) a typical cantilever blade. Also shown are the first-mode shapes for the three configurations. The frequencies and mode shapes shown in figure 1 were obtained from reference 6. Although the mode shapes for the hinged rigid-body modes are not influenced by rotational speed, the cantilever mode is altered somewhat by centrifugal stiffening, which reduces the curvature over the outboard portion of the blade and concentrates the curvature over the inboard portion of the blade. A comparison of the various mode shapes and natural frequencies for the flapwise degree of freedom at normal operating rotor rotational speed ($\Omega/\Omega_n = 1.0$) indicates that there is a marked similarity between the hinged and cantilever systems. The main point is that the mode shapes of the hinged blades and rotating cantilever blade are similar and the natural frequency ratio ω_{1R}/Ω_n for the three blades at operating rotational speed are at, or slightly above, a value of unity. Therefore, each type of blade has a natural frequency in flapping in close proximity to once per revolution of the rotor system.

From the standpoint of the blade forced response, the predominating force inputs are occurring once-per-rotor revolution. A typical source of such one-per-revolution force inputs is the aerodynamic force resulting from rotor cyclic control input. The governing equation of motion for the flapping-degree-of-freedom response to cyclic control input in hovering flight is derived in reference 5 and presented as equation (A1) in appendix A.

Substitution of the natural frequencies ω_{1R} and mode shapes w_{1R} at normal operating rotor speed from figure 1 into equations (A1) to (A6) gives the relative response characteristics of the hinged and cantilever blades. For blades that are assumed identical in uniform mass distribution and aerodynamic characteristics, the relative response characteristics are shown in figure 2. Each blade configuration is being forced at a frequency at or slightly below its natural frequency and the results indicate that the flapping motion response of each of the three blades is very nearly the same. Therefore, the rotating cantilever rotor blade deflects like a hinged blade and is far from being a rigid blade.

For the phase response of the three blades, the cantilever blade phase response is quite different from that of the hinged blades as shown in figure 2. The hinged blades have phase-angle response equal to or close to 90^o. However, the flapping deformation of the cantilever blade lags the force input by only 60^o to 70^o. The cantilever blade phase lag is far from that of a truly rigid rotor which would have a phase lag of 0^o. The reduced phase-angle response of the cantilever blade requires specific attention, otherwise the total rotor response to cyclic control input may be cross coupled. For example,

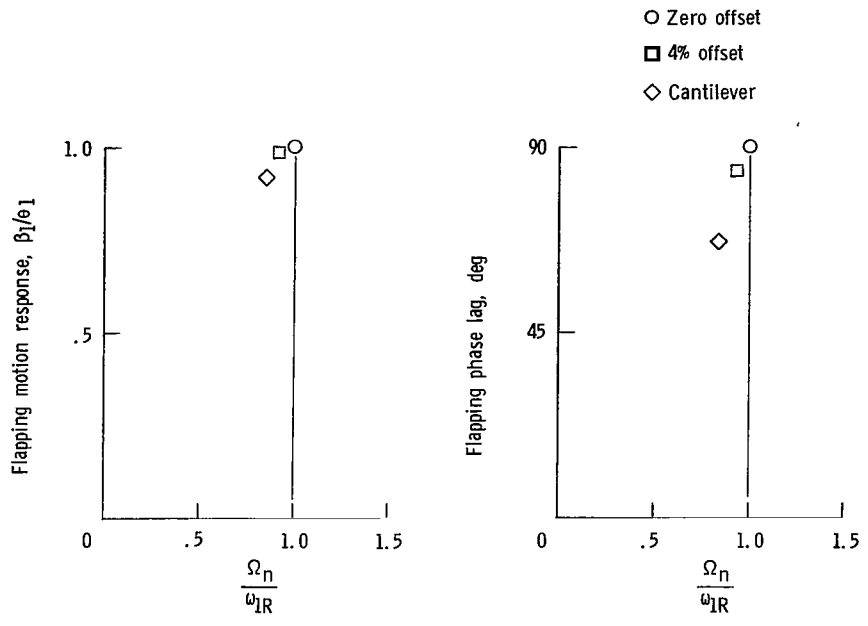

Figure 2.- Blade response to cyclic control input.

longitudinal cyclic control input B_1 produces a substantial lateral rotor-hub moment, as well as the desired direct longitudinal hub moment, unless the reduced phase-angle response of the cantilever blade is accommodated by proper control phasing. Therefore, the correct combination of A_1 and B_1 cyclic control is required to give a pure longitudinal hub moment.

Another area where the reduced phase-angle response of the hingeless rotor requires attention is in regard to rotor response to pitch and roll angular velocity. Here again, the force inputs to the blade associated with rotor angular velocity in pitch and roll originate from once-per-rotor-revolution gyroscopic and aerodynamic sources. The result is that the basic hingeless-rotor angular-velocity response is also cross coupled in the lateral and longitudinal directions. A longitudinal (pitching) angular velocity produces a lateral rotor moment as well as the desired direct longitudinal rotor moment (angular velocity damping moment). The presence of aircraft angular-velocity response cross coupling can adversely affect the rotor structural loads experienced in maneuvering flight. This problem is discussed in more detail in the section dealing with the analysis of maneuver loads encountered in flight. A number of important aspects of the influence of cross coupling on hingeless-rotor helicopter flying qualities are discussed in reference 4.

Equivalent System

In order to treat the dynamic response of the hingeless rotor system in a relatively simplified manner and to utilize conventional rotor analysis, the cantilever blade can be replaced by an equivalent offset hinge blade, which is considered as a rigid body, with spring restraint at the flapping and lagging hinges.

Flapping equivalence.- The equivalent flapping system arrangement is shown in figure 3. The equivalence is derived and described in reference 5. The virtual flapping hinge offset ξ_V and spring restraint K_{VF} are established on the basis of the cantilever-blade first-bending-mode shape, nonrotating natural frequency, and rotating natural frequency. The equivalent offset is selected to make the flapwise Southwell coefficient of the hinged blade equal to that of the cantilever blade. The general expression for the flapwise Southwell coefficient (refs. 5 and 6) is

$$K_{1F} = \frac{\omega_{1R}^2 - \omega_{1NR}^2}{\Omega^2} \tag{1}$$

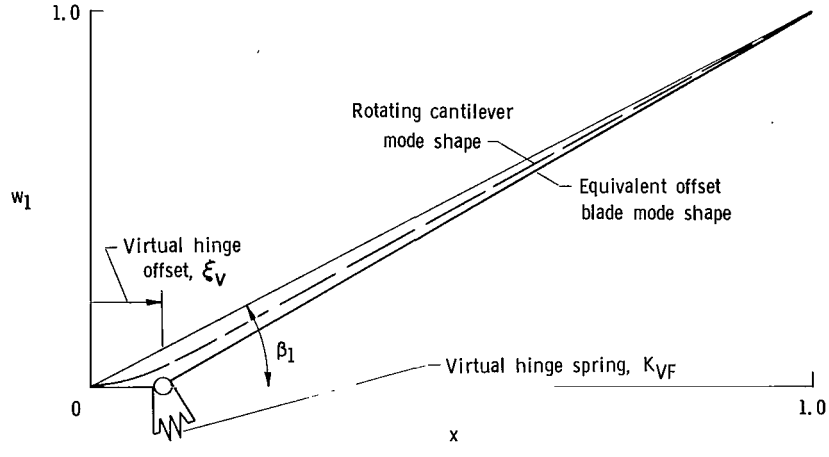

Figure 3.- Equivalent offset hinge blade with spring restraint.

For a uniform offset hinge blade the first-mode flapping Southwell coefficient in terms of basic blade parameters is

$$K_{1F} = 1 + \frac{e_V \sigma_V}{I_V} \tag{2}$$

Solving equation (2) for the nondimensional virtual hinge offset gives

$$\xi_V = \frac{e_V}{R} \approx \frac{2(K_{1F} - 1)}{3(2K_{1F} - 1)} \tag{3}$$

Substituting the cantilever-blade first-mode flapping Southwell coefficient into equation (3) gives the required virtual flapping hinge offset for the equivalent blade.

In order to provide complete dynamic equivalence some hinge spring restraint is required in addition to the hinge offset ξ_V. The spring constant K_{VF} is such as to give a nonrotating hinged-blade natural frequency ω_{1NR} equal to that of the nonrotating cantilever blade. The spring constant is given by

$$K_{VF} = I_V \omega_{1NR}^2 \tag{4}$$

This spring restraint at the hinge will be representative of the level of cantilever structural stiffness. For a typical case the contribution of this structural stiffness to the total rotating blade stiffness is about 5 percent of the total. The centrifugal force field provides 95 percent of the flapwise stiffening, even for the cantilever system. However, it is necessary to include the hinge spring in the equivalent blade treatment so that the blade flapping response phase angles and root bending moments of the cantilever blade can be simulated properly.

In general, the cantilever blade flapping response at normal operating rotor speed results in effective blade flapping angles β_1 which are very nearly equal to those of conventional offset hinged blades. However, at very low rotor rotational speed the structural stiffness of the cantilever blade plays the predominant role and serves to restrain the blade motions during starting and stopping of the rotor.

Lagging equivalence.- The virtual offset and spring restraint in the equivalent system lagging degree of freedom are established in the same manner as in the flapping degree of freedom. The general expression for the chordwise or lagging Southwell coefficient is defined as

$$K_{1L} \equiv \frac{\nu_{1R}^2 - \nu_{1NR}^2}{\Omega^2} \tag{5}$$

The general relationship between the flapwise and chordwise Southwell coefficients discussed in reference 7 is

$$K_{1L} \approx K_{1F} - 1 \tag{6}$$

The relation applies to both the cantilever and hinged rotor blades. Therefore, substituting equation (6) into equation (2) results in the following expression for the equivalent hinged blade lagging Southwell coefficient:

$$K_{1L} = \frac{e_V \sigma_V}{I_V} \tag{7}$$

Equating the expression in equation (7) to the chordwise Southwell coefficient for the hingeless rotor cantilever blade and solving for the offset result in

$$(\xi_V)_{\text{lagging}} \approx (\xi_V)_{\text{flapping}} \tag{8}$$

Therefore, for the equivalent system the virtual flapping and lagging hinges are considered to be coincident.

The virtual lag hinge spring restraint is

$$K_{VL} = I_V \nu_{1NR}^2 \tag{9}$$

Unlike the flapping spring, the lag spring represents a major portion of the total blade lagging stiffness because (1) the spring is simulating the high inherent chordwise structural stiffness of current hingeless blades and (2) there is reduced centrifugal force stiffening in the blade chordwise (or lagging) degree of freedom compared to the blade flapping degree of freedom.

Rotor Moment Characteristics

With the equivalent hinged blade virtual offset and spring restraint established on the basis of the cantilever blade characteristics, the cantilever blade root first-harmonic flapwise bending moments, chordwise bending moments, and effective flapping and lagging displacements can be calculated with conventional hinged-rotor analysis. The root moments and angular displacements calculated with the equivalent system are equal to those of the cantilever blade. This equivalence is derived in reference 5. In order to proceed with the analysis of the results of the hingeless-rotor flight investigation it is necessary to develop the general equations for calculating hingeless rotor-hub moments and first-harmonic blade chordwise structural bending moments.

Rotor-hub moments.- In contrast to the similarity in the amplitude of blade flapping motion, at normal operating rotor speed, a most significant difference between the hinged and cantilever blade is the magnitude of the once-per-rotor-revolution blade root moments developed simultaneously with blade flapping motion response. The effective

offset and spring restraint of the cantilever blade serve to develop large flapwise moments at the blade root. These blade root moments combine to give total rotor-hub moments which are an order of magnitude greater than those normally associated with conventional offset hinged rotor systems.

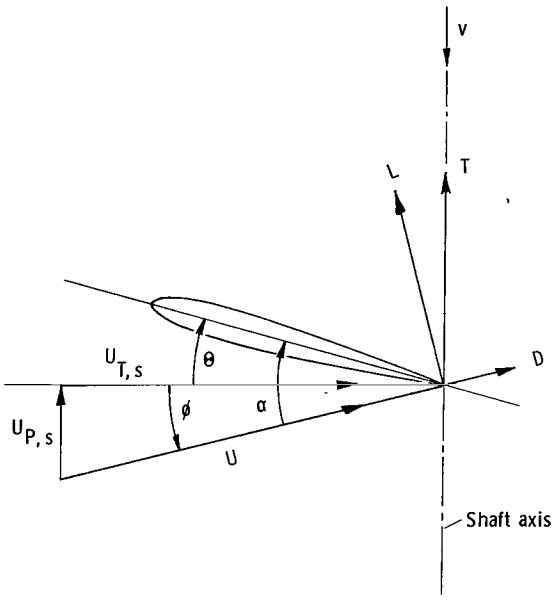

Figure 4.- Forces and velocities acting on a blade element.

The control-moment and angular-velocity damping-moment characteristics of a typical hingeless rotor system can be calculated by use of the conventional offset hinged-blade flapping equations, such as those given in reference 8, with suitable modifications to account for the hinge spring restraint. The hingeless rotor-hub moment equations are developed in this manner in appendix B. The force and velocity sign convention used in the development of these equations is shown in figure 4.

The results of sample calculations using the general equations from appendix B are shown in figures 5 and 6 for a three-blade rotor with an equivalent offset value of 10 percent. The longitudinal and lateral hub moment, in nondimensional form, are presented for a range of blade Lock number and blade nonrotating first-mode natural-frequency ratio ω_{1NR}/Ω. Current cantilever blade designs have a nonrotating flapwise frequency ratio ω_{1NR}/Ω on the order of 0.2.

Figure 5 indicates the relative magnitude of the direct longitudinal moment per degree of lateral blade cyclic feathering input and the associated lateral, or cross-coupled, moment. For a given value of ω_{1NR}/Ω the amount of cross coupling varies with blade Lock number γ due to the effect of aerodynamic damping on phase response. Figure 6 presents direct and cross-coupled rotor pitching-velocity damping-moment trends. Here again, the moment response is cross coupled and influenced by blade Lock number for any given value of ω_{1NR}/Ω.

The rotor control-moment and damping-moment capability indicated in figures 5 and 6, even for blades with low values of ω_{1NR}/Ω, are considerably greater than conventional helicopter rotor capability. The relative magnitude of hingeless and conventional articulated rotor-hub moment capability is indicated by the circle on the ordinate line of figures 5 and 6. This point represents the moment capability for a three-blade articulated rotor with a 4-percent hinge offset at a blade Lock number of 8. A teetering rotor system, which has no direct hub moment capability would lie at the origin of each

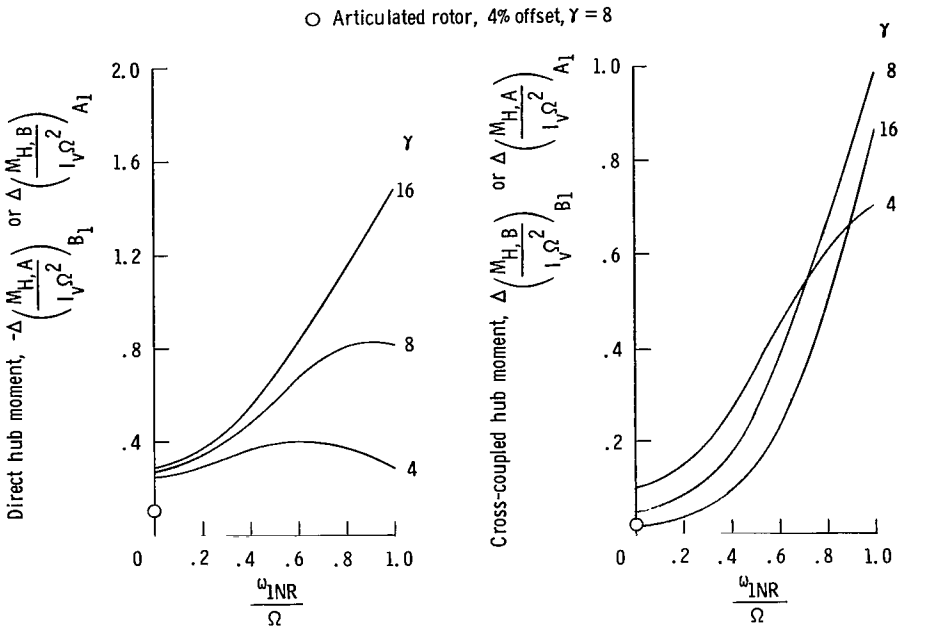

Figure 5.- Effect of blade stiffness and Lock number on rotor-hub control moment and cross coupling. $\varepsilon_v = 0.10$; three-blade rotor.

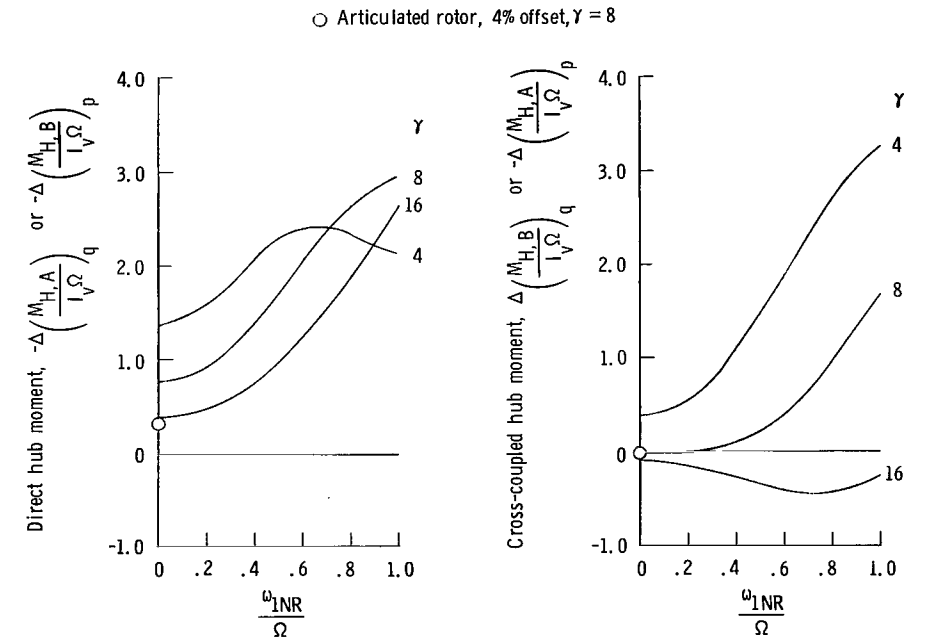

Figure 6.- Effect of blade stiffness and Lock number on rotor-hub damping moment and cross coupling. $\varepsilon_v = 0.10$; three-blade rotor.

figure. The additional aircraft moments developed as a result of rotor thrust vector tilt would be essentially the same for each rotor system, due to the similarity in the flapping response (rotor tilt) of the teetering, hinged, and hingeless rotors.

The increased moment capability of the hingeless rotor system has been confirmed by flight experience (ref. 4) and by wind-tunnel test results (ref. 9). This increased moment capability suggests that careful attention must be given to the blade root, rotor hub, rotor shaft, and pylon structural loads. The analytical and wind-tunnel results confirmed the need for an exploratory flight investigation to show the relative importance of various structural loads under actual operating conditions including maneuvers.

Blade chordwise bending moments.- A theoretical analysis of the oscillatory chordwise bending moments during maneuver conditions was performed by using an extension of the equivalent-offset hinged-blade analysis. The basic objective of the analysis was to gain some insight into the relationship between blade cyclic chordwise bending moments and the cyclic flapping, feathering, aircraft angular velocity, and aircraft angular acceleration. A parallel objective was to determine if the use of the equivalent offset blade with spring restraint could provide an adequate simulation of the fundamental cantilever dynamics to permit simple analytical treatment of the rotor structural loads.

The derivation of the chordwise structural bending-moment equation is presented in appendix C. The results of the analysis indicate that, for a given configuration, the blade oscillatory chordwise bending-moment buildup during maneuvers is primarily dependent upon the amplitude and phase relation between blade flapping deformation β_1, blade cyclic feathering motion θ_1, and aircraft angular velocity τ as indicated in equation (C20). The direct effects of aircraft angular velocity are small for practical values of τ. However, the effects of both aircraft angular velocity and angular acceleration are introduced indirectly through their influence on blade flapping motion, as indicated in equations (B25) and (B26).

FLIGHT INVESTIGATION

In order to proceed with an exploratory flight investigation with a hingeless rotor system, NASA obtained a duplicate of an existing set of experimental hingeless-rotor components. Because of fatigue considerations, the flight investigation of the experimental rotor system was restricted to a total flight time of 14 hours. The objective was to survey the dynamic, structural load, and flying qualities characteristics of the basic concept in order to define potential problem areas and to verify some of the predicted advantages attributed to the concept. The results of the flying qualities investigation are presented in reference 4.

Test Aircraft, Instrumentation, and Procedure

The experimental rotor configuration was identical to the rigid hub rotor described in reference 2. The test aircraft is shown in figure 7 and the aircraft physical parameters are given in table I. The basic aircraft was an Army OH-13G helicopter. The standard teetering rotor and the control linkage above the swash plate were removed and replaced by the experimental three-blade hingeless rotor system. The rotor blades were modified OH-13H helicopter metal blades mounted on an experimental rotor hub, as shown in figure 8. The hub was intentionally overdesigned to provide generous margins of safety. There was no intent to obtain an optimum rotor configuration. The test article represented an available experimental rotor basically fabricated from off-the-shelf components. The resulting configuration was designated as the XH-13N helicopter.

The principal feature of the main-rotor pitch control was the phasing used between the control inputs at the swash plate and the feathering axis of the rotor blades. This phasing was reduced from the usual 90^{o} to 62.5^{o} and corresponds to a control "retardation" of 27.5^{o}. This retardation, which was discussed in general in the section "Blade Flapping Response" in connection with cantilever blade response, was installed to eliminate control moment cross coupling. There was no attempt to eliminate the aerodynamic and gyroscopic cross coupling of rotor response to aircraft angular velocity. No artificial stabilization devices were used during the investigation and the horizontal stabilizer, normally used on the OH-13G aircraft, was removed prior to beginning the test program.

Figure 7.- Hingeless-rotor XH-13N helicopter. L-62-6643

TABLE I

TEST AIRCRAFT PHYSICAL PARAMETERS

Number of main-rotor blades	3
Main-rotor diameter	31.66 ft (9.65 m)
Main-rotor blade chord	11 in. (0.28 m)
Main-rotor blade weight	87 lb (387.15 N)
Built-in coning angle	2^{o}
Main-rotor blade airfoil	0015
Main-rotor blade twist	-7^{o}
Main-rotor blade Lock number, γ_V	3.85
Aircraft gross weight	2260 lb (10.057 kN)
Normal rotor rotational speed	344 rpm
Main-rotor solidity	0.055
Main-rotor blade calculated first-bending-mode natural frequencies:	
Flapwise	
Nonrotating	7 rad/sec
Rotating	40 rad/sec
Chordwise	
Nonrotating	41 rad/sec
Rotating	44 rad/sec

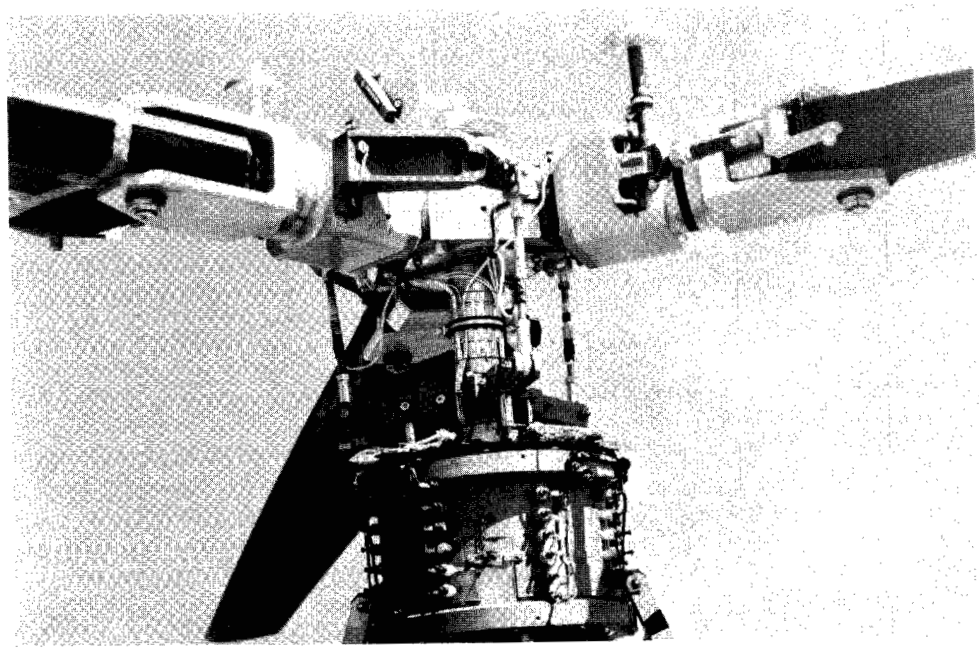

Figure 8.- Hingeless-rotor hub and slipring assembly. L-62-6644

Since the principal innovation in the hingeless-rotor-system concept is the capability to transfer large moments from the rotor system into the hub and rotor shaft, attention was focused on the measurement of the structural bending moments in this area. The blade root, hub, rotor shaft, and control linkages were the primary components selected for strain-gage instrumentation. Flight-test instrumentation was also installed for the measurement of the necessary parameters to document the aircraft flying qualities. These parameters included aircraft angular velocities and control positions. The installed research instrumentation was as follows:

Performance:
- Airspeed
- Altitude
- Engine manifold pressure

Flying qualities:
- Pitch angular velocity
- Roll angular velocity
- Yaw angular velocity
- Normal acceleration
- Longitudinal acceleration
- Lateral acceleration
- Pedal position
- Lateral stick position
- Longitudinal stick position
- Collective stick position

Structural loads:
- Main-rotor blade moments
  - Flapwise bending, station 41 (station 0 at rotor center line)
  - Flapwise bending, station 22
  - Chordwise bending, station 41
- Main-rotor hub
  - Flapwise bending moment, station 5
  - Drag link axial load
  - Chordwise bending moment, station 5
- Main-rotor blade pitch link axial load
- Main-rotor shaft
  - Shaft bending, station 17 (17 inches below plane of rotor blades) in phase with instrumented blade
  - Shaft bending, station 17, 90^{o} out of phase with instrumented blade
  - Shaft bending, station 30, in phase with instrumented blade

Engine mount:

Longitudinal engine mount rod axial load
Lateral engine mount rod axial load

Recorders:

36-channel NASA oscillograph
Angular velocity recorders
Pressure recorder
Acceleration recorder

As previously mentioned, the test program consisted of 14 hours of operation. During the program, data were obtained for various ground and flight operating conditions. In general, the flight conditions investigated included level flight throughout the forward speed range, autorotation, vertical descents, steep turns in level and autorotative flight, abrupt maneuvers, and slope take-offs and landings. The ground and flight operating conditions were

Ground run-up and shut-down
Lift-off and touch-down
Slope landings and take-offs
Hover in ground effect
Hover out of ground effect
Stick stirring in hover
Transition, accelerating from hover to forward speed
Transition, decelerating from forward speed to hover
Climbs
Descents, power-on
Autorotation, entries throughout speed range
Level flight to 70 knots
Rapid turns
Pull-ups
Partial power descents, up to 1400 ft/min
Control steps throughout speed range
Control pulses throughout speed range
Control reversals throughout speed range

Measured Structural Loads

The objective of the structural loads portion of this investigation was to sample all the practical ground and flight operating conditions in an effort to identify those conditions which require most immediate and detailed study. The rotor system possessed control capability of sufficiently large magnitude to cause concern over the

large-amplitude cyclic loadings that could be induced in the primary structure of the aircraft. The following discussion treats some of the more significant results of the structural loads investigation.

Ground operation.- The ground-operation investigation was limited to observing the trends in the rotor-blade and rotor-shaft bending moments. Since the rotor shaft was designed for use with a teetering rotor system, the allowable cyclic bending-moment amplitude was established at 1500 ft-lb (2034.54 m-N) on the basis of rotor-shaft fatigue test data. This allowable cyclic shaft moment was incompatible with the much higher moments that could be developed with the experimental hingeless-rotor system. The hingeless-rotor system had the capability of producing hub moments on the order of 1200 ft-lb/deg (1627.63 m-N/deg) of cyclic control input; therefore, extreme care had to be exercised by the pilot to keep the cyclic stick centered during ground run-up and lift-off. It was necessary for the pilot to anticipate the cyclic trim position during transition from the ground to the airborne condition in order to avoid large transients in rotor-shaft cyclic bending moment.

The probability of encountering large magnitude rotor-shaft bending stresses is recognized as a problem requiring attention but is not considered a critical problem. The direct approach to alleviate the problem is to provide a short rotor shaft of sufficient diameter to accommodate the moments that can be developed by the rotor system. In any detailed design of complete hingeless-rotor helicopter this approach would require only a low weight penalty.

Structural loads were also observed during slope take-offs and landings. Here again the results were restricted by the allowable rotor shaft loads. However, it was determined that the best control technique to minimize cyclic bending moments in the rotor system was to apply almost full collective control prior to bringing the aircraft to a level attitude with cyclic control. The reverse control sequence was used in slope landings. In addition to pilot technique and rotor shaft design, there are a number of available approaches toward the reduction of the rotor shaft bending stresses, such as reducing gear tread width, but these require specific design attention.

Level flight.- The level-flight structural loads in primary rotor components are summarized in figure 9. Although the test rotor was fabricated from standard articulated components (except for the hub), the measured loads experienced in level flight throughout the speed range were not above the design "fatigue limit" for these components. Fatigue limit is defined as the cyclic load amplitude which results in a fatigue life equal to 10^8 cycles. Although the pitch link loads appear to be the largest in relative magnitude in figure 9, they were not considered to be unusually high. The maximum continuous cyclic pitch link load during transition was of the order of ±80 lb (356 N), with a zero mean load. In this case, the stress levels can be reduced without difficulty by a slight increase in pitch link cross-sectional area.

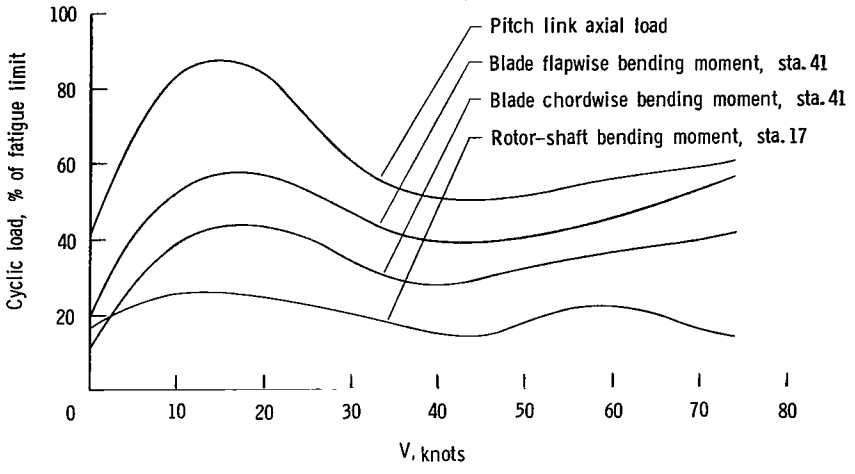

Figure 9.- Hingeless-rotor cyclic structural loads in level flight.

Maneuver flight.- During the test program, structural loads were monitored carefully as the flight envelope was expanded in order to assure safety of flight. In general, the high loadings were not of a critical nature, and the increase in load level with severity of the maneuver was certainly not unexpected, especially with regard to rotor shaft and blade flapwise bending moments. The structural loading found to be of most concern was the "in-plane" or chordwise bending moments induced in the rotor blades. The amplitude of the rotor-blade chordwise cyclic bending moment was very sensitive to maneuvers in which high aircraft angular velocities were developed. In some instances the amplitude of this loading expanded well beyond the structural fatigue limit, during pitch and roll maneuvers that were well within the control capability of the aircraft. The buildup of cyclic chordwise blade bending moment occurred in pitch and roll maneuvers in hover and throughout the forward speed range.

Maneuver in hover: The sample loads measurements presented in time-history form in figure 10 are for a hover maneuver where the pilot executed a longitudinal control step displacement and recovery. Also presented in figure 10 are the measured histories of longitudinal and lateral control displacement, pitch angular velocity, and blade feathering motion. During the period of maximum pitching angular velocity, the buildup of the cyclic chordwise bending moment reaches a maximum amplitude of ±29 000 in-lb (3275 m-N), which is above the structural fatigue limit of the blade. The oscillatory flapwise bending moments increased in amplitude during the recovery maneuver, but did not show the degree of sensitivity to the maneuver exhibited by the chordwise bending moment. The rotor-shaft cyclic moments during the initial portion of the maneuver do not build up because the initial control moment cancels a rotor-shaft moment resulting from minor center-of-gravity offset. However, during the recovery portion of the

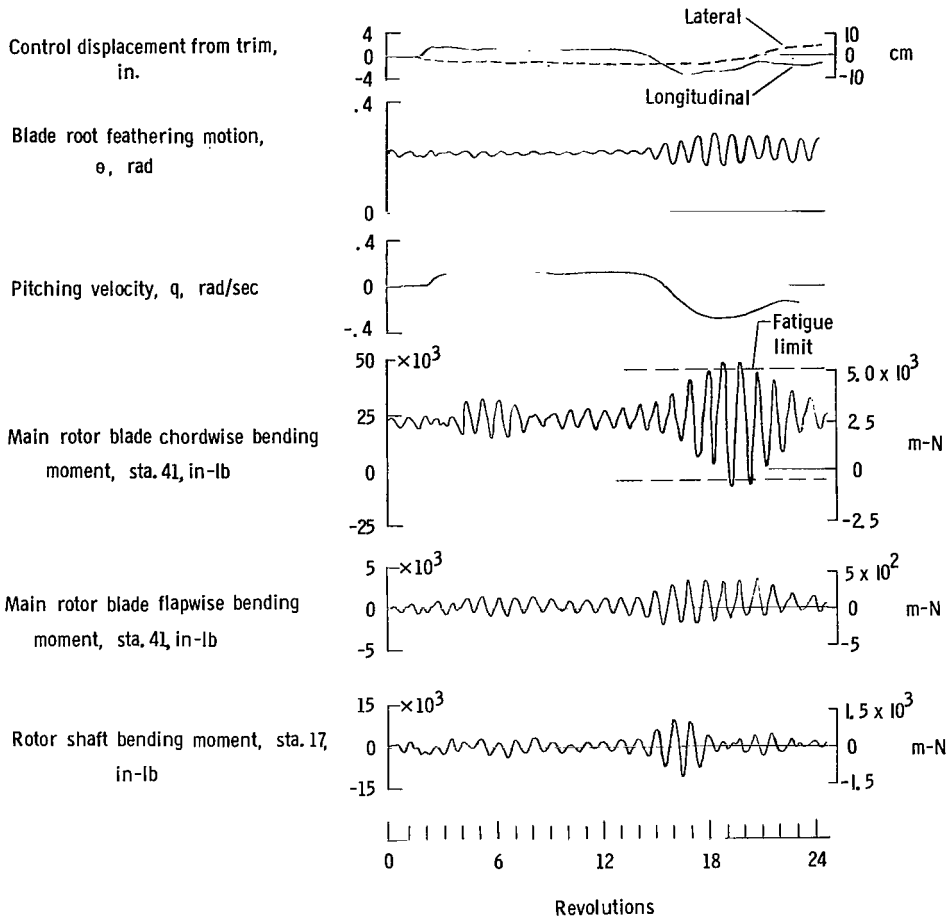

Figure 10.- Structural-loads history during pitching maneuver and recovery with hingeless-rotor helicopter in hovering flight. Rotor speed, 344 rpm.

maneuver, where the control moment and the offset center-of-gravity moment add, the rotor-shaft cyclic moments reach a maximum at a period of maximum angular acceleration.

Maneuver at 70 knots: The situation at a forward speed of 70 knots is shown in figure 11. Again the blade chordwise bending moment shows the large buildup during the rolling maneuver and again the amplitude is above the structural fatigue limit. Continuous operation at the maximum chordwise bending-moment amplitude of 40 000 in-lb (4515 m-N) would result in a 10-hr fatigue life for this rotor blade; this indicates the significance of the load levels that can be encountered in the maneuvers. The point here is that the maneuvers in which the high chord loads are encountered are well within the operational capability of the helicopter equipped with a hingless rotor system.

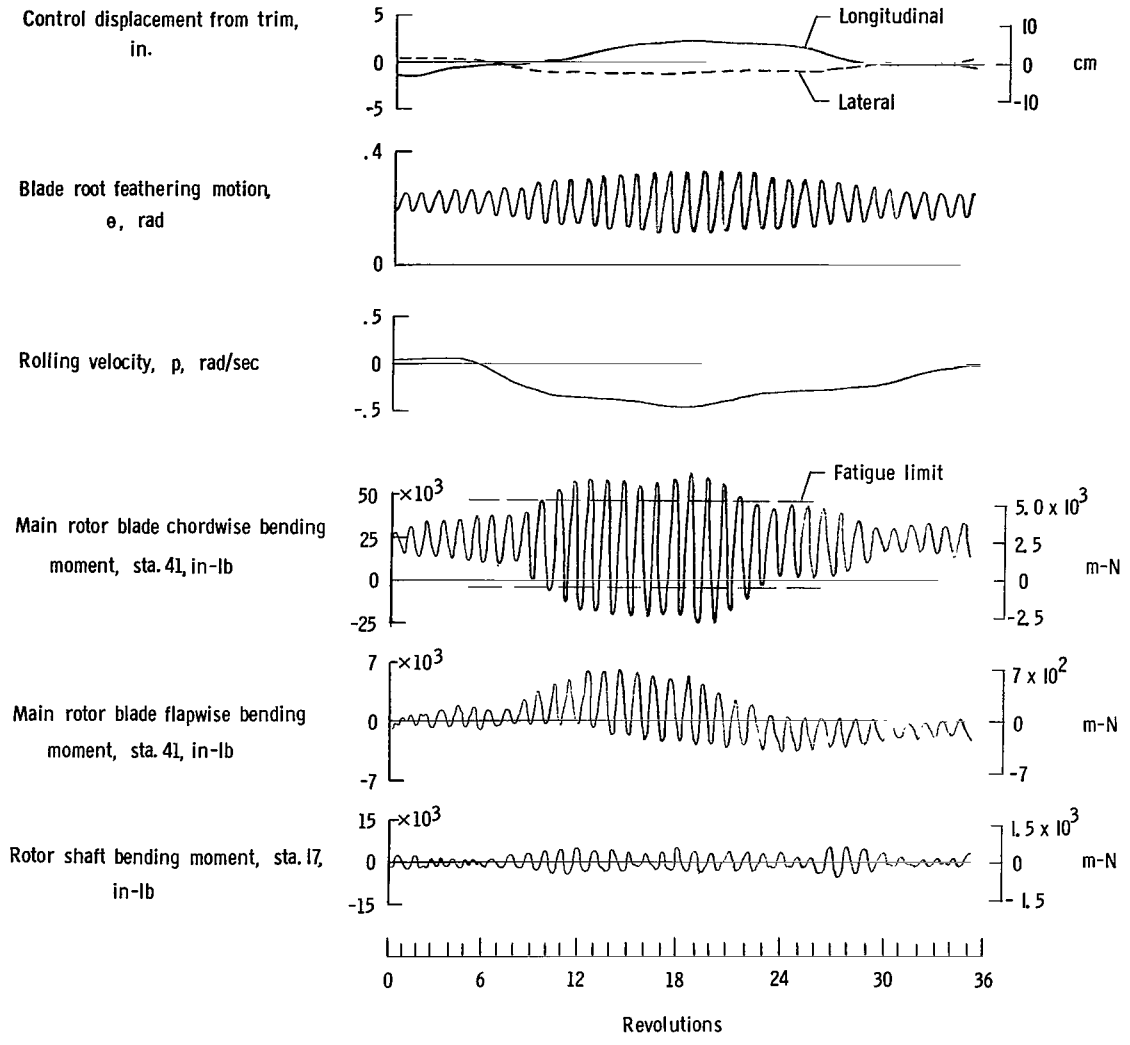

Figure 11.- Structural-loads history during rolling maneuver with hingeless-rotor helicopter in level flight at a forward speed of 70 knots. Rotor speed, 344 rpm.

Maneuver in autorotation: In contrast to the structural loads measured in the hovering and the 70-knot maneuver conditions are the loads measured during a rolling maneuver performed in autorotation. This case is shown in figure 12. The entry speed into this autorotation was approximately 45 knots. There is a complete lack of buildup in blade chordwise cyclic bending-moment amplitude during the maneuver, even though an aircraft angular velocity of 0.4 rad/sec was obtained.

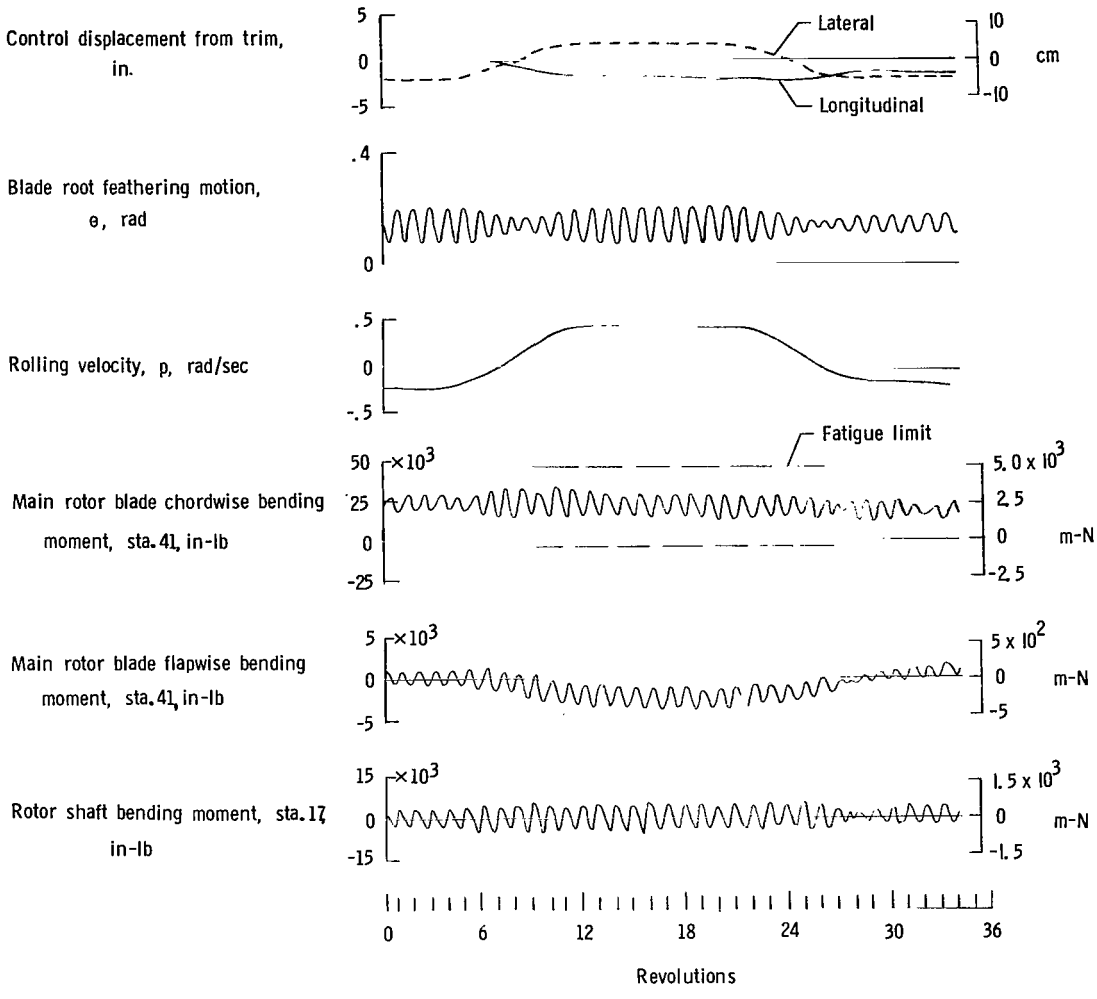

Figure 12.- Structural-loads history during rolling maneuver with hingeless-rotor helicopter in autorotation. Entry speed, 45 knots; rotor speed, 344 rpm.

Analysis of Blade Chordwise Moments in Maneuvers

From the standpoint of structural loads, the sensitivity of the blade cyclic chordwise bending-moment amplitude to maneuvers was the primary concern in the flight investigation. A comparison was made between measured and calculated chordwise moment amplitude and azimuth phase angle. This comparison was undertaken to clarify the basic cause of the buildup of chordwise structural loads in maneuvers and to determine what might be done to alleviate this problem. The equations developed in appendix C were utilized in the analysis. This analysis includes only the aerodynamic effects of blade twist. Equation (C20) was used to calculate detailed histories of blade cyclic chordwise bending-moment amplitude and phase angle for the hovering and 70-knot

maneuvers. A qualitative analysis of the noncritical autorotation maneuver was also performed.

The calculation of cyclic chordwise bending moments is dependent upon the blade flapping β_1 as indicated in equation (C20). The theoretical calculation of the relatively low magnitude cyclic flapping motion during the maneuvers was evaluated and the results indicated that steady-state flapping can be calculated with accuracy on the order of 15 percent using equations (B26) and (B27). However, satisfactory prediction of blade cyclic flapping amplitude and azimuth phasing throughout a specific transient maneuver for use in equation (C20) requires a higher degree of accuracy. In order to avoid compounding errors by calculating β_1 as an input to equation (C20) the measured cyclic flapping moments were used to determine effective flapping motion β_1.

The conversion from measured first harmonic bending moment to effective equivalent blade flapping angle β_1 was accomplished on the basis of the moment equivalence established between the cantilever blade and virtual hinge offset blade. Specifically, the bending-moment distributions associated with a given first-mode flapping response β_1 of the cantilever blade and the equivalent offset hinge blade are equal at the rotor center line. The first-harmonic bending moment measured at any given cantilever blade station can be related to the moment at the rotor center line through the use of the normalized first-mode bending-moment distribution. In turn, the rotor center line moment is associated with a given blade flapping amplitude β_1. This same technique was used in the lagging degree of freedom to convert from calculated equivalent blade moments M_{VL} to cantilever blade moments $M_{c,1}$ at a specific blade station.

Maneuver in hover.- The comparison between measured and calculated first-harmonic chordwise bending moment and azimuth phase angle is shown in figure 13 for the hovering maneuver illustrated in figure 10. The agreement between the measured and calculated time histories is satisfactory and indicates that the equivalent blade analysis is adequate for a preliminary assessment of hingeless-rotor blade structural loads during a hovering maneuver.

An example of how the flapping deformations and feathering motions combine to give large-amplitude chordwise bending moments is illustrated in figure 14. This figure is a polar plot of the situation at the time of maximum chordwise moment amplitude indicated in figure 13 by the vertical line and symbols at time $t = 4.4$ sec. This polar display is a depiction of the relative amplitude and phasing of the calculated feathering and flapping contributions to the chordwise bending moment. The measured and calculated resultant chordwise bending-moment amplitude and phasing is also indicated in figure 14. The moments in figure 14 are nondimensionalized on the basis of the maximum measured chordwise moment amplitude.

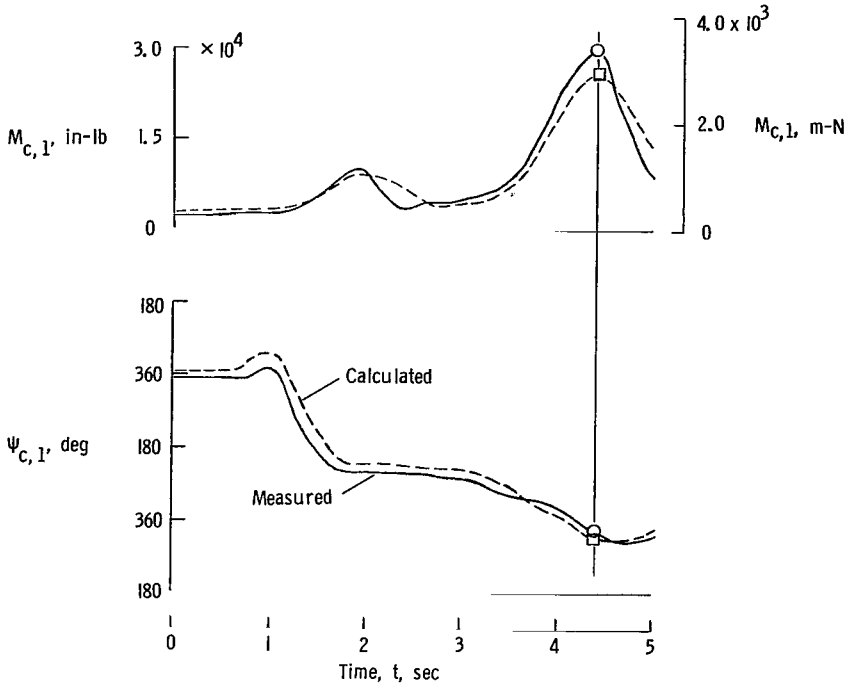

Figure 13.- Comparison of measured and calculated chordwise bending moments at blade station 45 during hovering pitch maneuver.

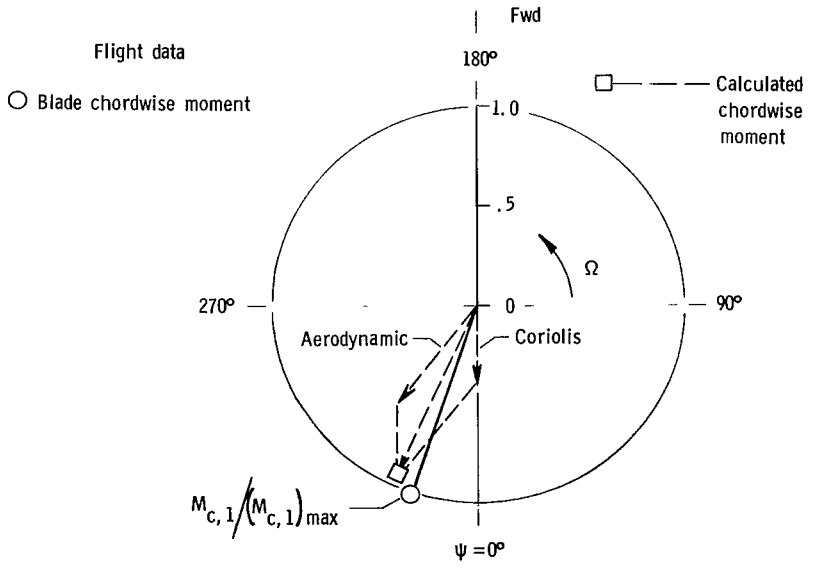

Figure 14.- Maximum blade cyclic chordwise bending moments in hovering pitching maneuver. t = 4.4 sec.

The direct aerodynamic induced chordwise moment caused by control input is in-phase with the feathering motion at $\psi = 320^{o}$. The cyclic chordwise moment induced by blade flapping motion in this particular case is at an azimuth position of $\psi = 0^{o}$. This $\psi = 0^{o}$ component of chordwise moment is the result of lateral blade flapping displacement at $\psi = 270^{o}$, which in turn is the direct result of cross-coupled response to the basic pitching maneuver. The resulting blade flapping velocity takes place at $\psi = 0^{o}$ and induces chordwise moments through Coriolis effects. The aerodynamic induced chordwise moments associated with flapping velocity are negligible in this case.

The resultant vector sum of the calculated aerodynamic and Coriolis induced chordwise moment occurs at an azimuth angle of 355^{o}; this agrees reasonably well with the measured maximum cyclic chordwise moment. The comparison of measured and calculated moments verifies the relation indicated by equation (C20) which states that the chordwise moments result primarily from blade flapping β_1 and feathering θ_1 associated with the maneuver. The situation is aggravated by the unfavorable phasing of blade flapping and feathering caused by the cross-coupled moment response of the rotor.

Maneuvers in forward flight.- An analytical check on the direct effect of a moderate forward velocity on the maneuver induced chordwise moment buildup indicated that the effects were secondary for low tip speed rotors. Therefore, the hovering analysis was also applied to the 70-knot case shown in figure 11. The comparison of measured and calculated cyclic chordwise bending-moment amplitude and azimuth phasing is shown in figure 15. The comparison indicates that reasonable agreement is obtained when extending the hovering analysis to the 70-knot case. The results indicated in this single case may be fortuitous, since the situation is certainly an overextension of a hovering analysis.

Qualitative examination of the autorotation case, shown in figure 12, indicated that the theory would predict low amplitude cyclic chordwise moments in the maneuver. This result is in agreement with the measured results.

Methods for Alleviation of the Problem

Since the cross coupling of rotor moment in the transient maneuvers contributes to the buildup of blade cyclic chordwise moments, every effort should be made to minimize the cross coupling associated with aircraft angular velocity. This is obviously desirable from the standpoint of control response as well as for the relief of rotor structural loads. However, the elimination of cross coupling associated with aircraft angular velocity cannot be counted upon to eliminate unfavorable β_1 and θ_1 phasing in all transient maneuvers.

The results of the flight investigation and analysis indicate that the problem is inherent in hingeless rotors utilizing blades which are stiff in the chordwise direction.

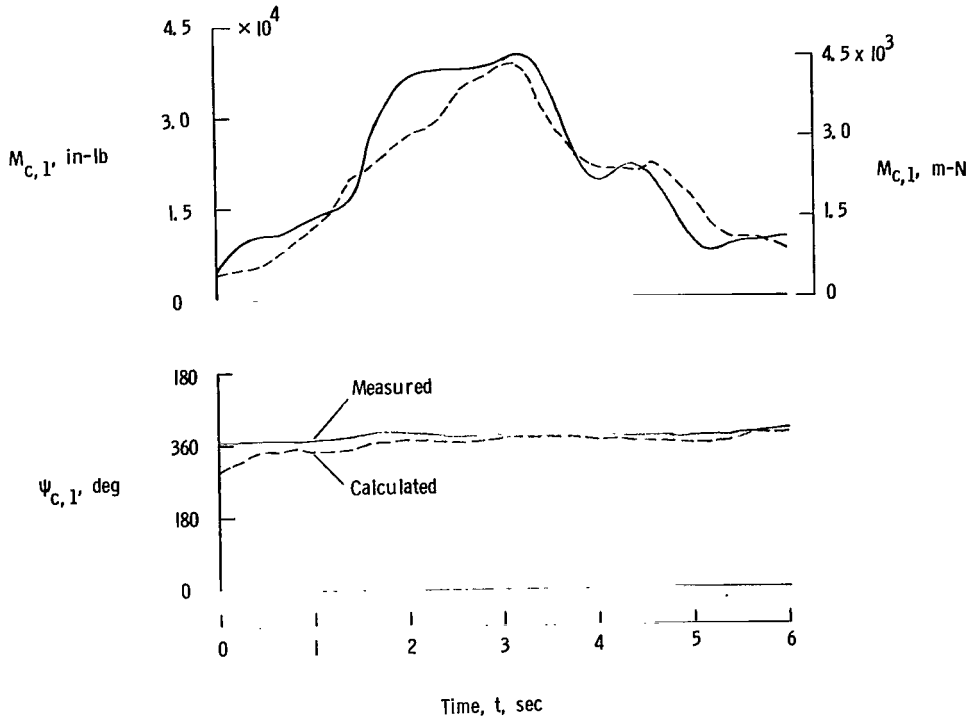

Figure 15.- Comparison of measured and calculated chordwise bending moments at blade station 45 during a rolling maneuver at 70 knots.

A more direct method of solution is to introduce chordwise blade flexibility which, in effect, reduces the value of K_{VL} in equation (C20). Sufficient flexibility must be introduced to assure that the blade chordwise natural frequency is lowered to a value sufficiently below normal rotor rotation speed to avoid unnecessary resonant amplification of the blade chordwise response. Basically, the reduced stiffness in the chordwise degree of freedom allows centrifugal relief of the blade structural bending moments just as in the flexible flapwise degree of freedom. The feasibility of introducing chordwise flexibility to reduce chordwise cyclic bending moments is discussed in reference 10. The data which support this approach are from the results of the dynamic model wind-tunnel investigation reported in reference 11.

The preliminary results of a current flight research investigation utilizing the XH-51N hingeless-rotor helicopter indicate the same basic trends in rotor system structural loads as noted in the XH-13N investigation. Reference 12 summarizes the preliminary results and compares them with the pertinent XH-13N results. In general the XH-51N and XH-13N show the same relative magnitude of level flight and maneuver flight cyclic bending moments at the rotor blade root. In both cases the maneuver loads are significantly higher than the level flight loads throughout the speed range.

CONCLUSIONS

The exploratory flight investigation and analysis of hingeless-rotor system structural loads has led to the following conclusions:

1. With the exception of rotor blade chordwise bending moments, the rotor system structural loads experienced during the flight investigation, including rapid maneuvers, were not considered to be inherently critical for the hingeless rotor system.

2. The structural load of most concern, which is inherent in hingeless rotors using stiff chordwise blades of conventional design, was the oscillatory blade chordwise bending moment. The amplitude of this moment was extremely sensitive to aircraft maneuvers throughout the speed range.

3. A simplified analytical treatment of the rotor hub moments and cantilever blade bending moments was performed by utilizing an extension of the concept of an equivalent virtual offset blade with spring restraint. This approach resulted in reasonable correlation with the measured results in hover and at moderate tip-speed ratios.

4. The results of the investigation indicate that at normal rotor rotational speed the centrifugal force field provides approximately 95 percent of the cantilever blade stiffening in the flapwise degree of freedom. Thus, the cantilever blade deflects in the first flapwise mode an amount virtually equal to a hinged blade and simultaneously provides rotor hub moments which are significantly greater than those obtainable from articulated rotor systems.

5. In order to make preliminary assessments of hingeless rotor blade motions and rotor moment capability it appears feasible to modify conventional offset-hinge rigid-blade techniques by the addition of the proper virtual spring restraint at the flapping and lagging hinges. The spring restraint and hinge offset are determined on the basis of the cantilever blade dynamic characteristics.

Langley Research Center,
National Aeronautics and Space Administration,
Langley Station, Hampton, Va., June 7, 1966.

APPENDIX A

HELICOPTER ROTOR BLADE FLAPPING RESPONSE TO CYCLIC FEATHERING INPUT IN HOVERING FLIGHT

The governing equation of motion for the flapping response of a rotating blade due to cyclic feathering input is given in reference 5 as:

$$\frac{d^2\beta_1}{d\psi^2} + \frac{\gamma}{8}\left(\frac{4}{3}\frac{\int_0^1 x\bar{w}_{1R}{}^2 dx}{\int_0^1 \bar{w}_{1R}{}^2 dx}\right)\frac{d\beta_1}{d\psi} + \left(\frac{\omega_{1R}}{\Omega}\right)^2 \beta_1 \approx \frac{\gamma}{8}\left(\frac{4}{3}\frac{\int_0^1 x^2\bar{w}_{1R}\, dx}{\int_0^1 \bar{w}_{1R}{}^2 dx}\right)\theta_1 \sin\left(\Omega t - \psi_{\theta,1}\right) \quad \text{(A1)}$$

where

$$\bar{w}_{1R} = \frac{w_1}{R}$$

Therefore,

$$\frac{\beta_1}{\theta_1} = \Gamma_{\beta,1}\frac{\beta_{1,\text{static}}}{\theta_1} \quad \text{(A2)}$$

$$\frac{\beta_{1,\text{static}}}{\theta_1} = \frac{\gamma}{8}\left(\frac{\Omega}{\omega_{1R}}\right)^2\left(\frac{4}{3}\frac{\int_0^1 x^2\bar{w}_{1R}\, dx}{\int_0^1 \bar{w}_{1R}{}^2 dx}\right) \quad \text{(A3)}$$

$$\Gamma_{\beta,1} = \left\{\left[1 - \left(\frac{\Omega}{\omega_{1R}}\right)^2\right]^2 + 4\delta_1{}^2\left(\frac{\Omega}{\omega_{1R}}\right)^2\right\}^{-1/2} \quad \text{(A4)}$$

$$\delta_1 = \frac{\gamma}{16}\left(\frac{\Omega}{\omega_{1R}}\right)\left(\frac{4}{3}\frac{\int_0^1 x\bar{w}_{1R}{}^2 dx}{\int_0^1 \bar{w}_{1R}{}^2 dx}\right) \quad \text{(A5)}$$

$$\Phi_{\beta,1} = \tan^{-1}\left[\frac{2\delta_1\left(\frac{\Omega}{\omega_{1R}}\right)}{1 - \left(\frac{\Omega}{\omega_{1R}}\right)^2}\right] \quad \text{(A6)}$$

APPENDIX B

DERIVATION OF HINGELESS-ROTOR HUB MOMENT EQUATIONS FOR HOVER FLIGHT USING EQUIVALENT HINGED BLADE ANALYSIS

The equivalent uniform blade hinge offset ξ_v and hinge spring restraint K_{VF} for a given hingeless-rotor cantilever blade configuration can be established by using equations (3) and (4). The summation of the once-per-rotor-revolution moments about the virtual flapping hinge is

$$\sum M_{VF} = M_{T,F} + M_{CF,F} + M_{I,F} + M_{G,F} + M_{AA,F} + M_{S,F} = 0 \tag{B1}$$

The expression for blade centrifugal force flapping moment is

$$M_{CF,F} = -\Omega^2\beta_1\left(I_v + e_v\sigma_v\right) \tag{B2}$$

The expression for blade inertia flapping moment is

$$M_{I,F} = -I_v\ddot{\beta}_1 \tag{B3}$$

The independent variable can be changed from t to ψ as follows:

$$\left.\begin{aligned}\dot{\beta} &= \Omega\frac{d\beta_1}{d\psi} = \Omega\bar{\beta}_1 \\ \ddot{\beta} &= \Omega^2\frac{d^2\beta_1}{d\psi^2} = \Omega^2\bar{\bar{\beta}}_1\end{aligned}\right\} \tag{B4}$$

and equation (B3) becomes

$$M_{I,F} = -I_v\bar{\bar{\beta}}_1 \tag{B5}$$

The expression for blade flapping moment due to gyroscopic forces induced by aircraft angular velocity is

$$M_{G,F} = 2\Omega\bar{\tau}\left(I_v + e_v\sigma_v\right) \tag{B6}$$

where

$$\bar{\tau} = p \cos \psi - q \sin \psi$$

The expression for blade flapping moment due to aircraft angular acceleration is

$$M_{AA,F} = -\dot{\tau}\left(I_V + e_V \sigma_V\right) \tag{B7}$$

where

$$\dot{\tau} = -\dot{q} \cos \psi - \dot{p} \sin \psi$$

The expression for blade flapping moment due to the flapping hinge spring is

$$M_{S,F} = -K_{VF} \beta_1 \tag{B8}$$

If the aerodynamic drag moment is neglected, the expression for the thrust moment may be written with the aid of figure 4 as

$$M_{T,F} = \int_{e_V}^{BR} \frac{1}{2} \rho U^2 c (r - e_V) c_l \, dr \tag{B9}$$

Let

$$\left.\begin{aligned} x &= \frac{r}{R} \\ \xi_V &= \frac{e_V}{R} \\ u &= \frac{U}{\Omega R} \\ c_l &= a\alpha \end{aligned}\right\} \tag{B10}$$

Substituting equations (B10) into equation (B9) gives

$$M_{T,F} = \frac{1}{2} k_3 \rho a c \Omega^2 R^4 \int_0^1 u^2 x \alpha \, dx \tag{B11}$$

where

$$\left.\begin{aligned} k_3 &= \left(B^4 - \frac{4}{3}B^3\xi_v\right) \\ u &\approx x \end{aligned}\right\} \tag{B12}$$

The inflow angle may be found from the following equations:

$$\phi = \tan^{-1}\frac{U_{P,s}}{U_{T,s}} \tag{B13}$$

$$U_{P,s} = -v - r\dot{\beta} + qr\cos\psi + pr\sin\psi \tag{B14}$$

$$U_{T,s} = \Omega r \tag{B15}$$

The section angle of attack can be found from the following relation:

$$\begin{aligned} \alpha &= \Theta + \phi \\ &= \theta_o + \theta_t x - A_1\cos\psi - B_1\sin\psi + \phi \end{aligned} \tag{B16}$$

The first-harmonic thrust moment about the virtual flapping hinge is

$$M_{T,F} = \frac{1}{8}k_3\gamma_v I_v\Omega^2\left(-A_1\cos\psi - B_1\sin\psi - \bar{\beta}_1 + \frac{q}{\Omega}\cos\psi + \frac{p}{\Omega}\sin\psi\right) \tag{B17}$$

where

$$\gamma_v = \frac{\rho acR^4}{I_v} \tag{B18}$$

Substituting these moments into equation (B1) and dividing by $I_v\Omega^2$ gives the general first-harmonic flapping equation of motion as follows:

$$\begin{aligned} &k_3\frac{\gamma_v}{8}\left(-A_1\cos\psi - B_1\sin\psi - \bar{\beta}_1 + \frac{q}{\Omega}\cos\psi + \frac{p}{\Omega}\sin\psi\right) - \ddot{\bar{\beta}}_1 - K_{1F}\beta_1 - 2K_{1F}\frac{q}{\Omega}\sin\psi \\ &+ 2K_{1F}\frac{p}{\Omega}\cos\psi + K_{1F}\frac{\dot{q}}{\Omega^2}\cos\psi + K_{1F}\frac{\dot{p}}{\Omega^2}\sin\psi - \left(\frac{\omega_{1NR}}{\Omega}\right)^2\beta_1 = 0 \end{aligned} \tag{B19}$$

where

$$K_{1F} = 1 + e_v \frac{\sigma_v}{I_v} \tag{B20}$$

and

$$\left.\begin{aligned} \beta_1 &= -a_1 \cos\psi - b_1 \sin\psi \\ \bar{\beta}_1 &= a_1 \sin\psi - b_1 \cos\psi \\ \bar{\bar{\beta}}_1 &= a_1 \cos\psi + b_1 \sin\psi \end{aligned}\right\} \tag{B21}$$

Equating $\sin\psi$ terms gives:

$$a_1 = \Gamma_F \left\{ -B_1 + \frac{p}{\Omega} - \frac{8K_{1F}}{k_3\gamma_v}\left(\frac{2q}{\Omega} - \frac{\dot{p}}{\Omega^2}\right) + \left[K_{1F} - 1 + \left(\frac{\omega_{1NR}}{\Omega}\right)^2\right]\frac{8}{k_3\gamma_v}\left(A_1 - \frac{q}{\Omega} - \frac{16K_{1F}}{k_3\gamma_v}\frac{p}{\Omega} - \frac{8K_{1F}}{k_3\gamma_v}\frac{\dot{q}}{\Omega^2}\right)\right\} \tag{B22}$$

Equating the $\cos\psi$ terms gives:

$$b_1 = \Gamma_F \left\{ A_1 - \frac{q}{\Omega} - \frac{8K_{1F}}{k_3\gamma_v}\left(\frac{2p}{\Omega} + \frac{\dot{q}}{\Omega^2}\right) + \left[K_{1F} - 1 + \left(\frac{\omega_{1NR}}{\Omega}\right)^2\right]\frac{8}{k_3\gamma_v}\left(B_1 - \frac{p}{\Omega} + \frac{16K_{1F}}{k_3\gamma_v}\frac{q}{\Omega} - \frac{8K_{1F}}{k_3\gamma_v}\frac{\dot{p}}{\Omega^2}\right)\right\} \tag{B23}$$

where

$$\Gamma_F = \left\{\left[K_{1F} - 1 + \left(\frac{\omega_{1NR}}{\Omega}\right)^2\right]^2\left(\frac{8}{k_3\gamma_v}\right)^2 + 1\right\}^{-1} \tag{B24}$$

The longitudinal flapping motion increments due to cyclic feathering, aircraft angular velocity, and aircraft angular acceleration are as follows:

APPENDIX B

$$
\left.
\begin{aligned}
\frac{\Delta a_1}{A_1} &= \left\{\left[K_{1F} - 1 + \left(\frac{\omega_{1NR}}{\Omega}\right)^2\right]\frac{8}{k_3\gamma_v}\right\}\Gamma_F \\
\frac{\Delta a_1}{B_1} &= -\Gamma_F \\
\frac{\Delta a_1}{q} &= -\frac{16}{k_3\gamma_v\Omega}\left\{K_{1F} + \frac{1}{2}\left[K_{1F} - 1 + \left(\frac{\omega_{1NR}}{\Omega}\right)^2\right]\right\}\Gamma_F \\
\frac{\Delta a_1}{p} &= \frac{1}{\Omega}\left\{1 - \left[K_{1F} - 1 + \left(\frac{\omega_{1NR}}{\Omega}\right)^2\right]\frac{128K_{1F}}{(k_3\gamma_v)^2}\right\}\Gamma_F \\
\frac{\Delta a_1}{\dot{q}} &= -\left\{\left[K_{1F} - 1 + \left(\frac{\omega_{1NR}}{\Omega}\right)^2\right]\left(\frac{8}{k_3\gamma_v}\right)^2 K_{1F}\right\}\Gamma_F \\
\frac{\Delta a_1}{\dot{p}} &= \left\{\frac{8K_{1F}}{k_3\gamma_v\Omega^2}\right\}\Gamma_F
\end{aligned}
\right\} \qquad \text{(B25)}
$$

The lateral flapping motion increments due to cyclic feathering, aircraft angular velocity, and aircraft angular acceleration are as follows:

$$
\left.
\begin{aligned}
\frac{\Delta b_1}{B_1} &= \frac{\Delta a_1}{A_1} \\
\frac{\Delta b_1}{A_1} &= -\frac{\Delta a_1}{B_1} \\
\frac{\Delta b_1}{p} &= \frac{\Delta a_1}{q} \\
\frac{\Delta b_1}{q} &= -\frac{\Delta a_1}{p} \\
\frac{\Delta b_1}{\dot{p}} &= \frac{\Delta a_1}{\dot{q}} \\
\frac{\Delta b_1}{\dot{q}} &= -\frac{\Delta a_1}{\dot{p}}
\end{aligned}
\right\} \qquad \text{(B26)}
$$

APPENDIX B

The structural bending moment transmitted across the virtual flapping hinge is

$$M_{VF} = K_{VF}\beta_1 \tag{B27}$$

The total hub moment at the rotor center is

$$M_H = \frac{n}{2}\left(M_{VF} + e_V S_{VF}\right) \qquad (n > 2) \tag{B28}$$

The first harmonic hub moments due to shear offset are developed in the same manner as the flapping moments about the virtual hinge. This development is as follows:

$$\sum e_V S_{VF} = \left(S_{T,F} + S_{I,F} + S_{G,F} + S_{AA,F}\right)e_V \tag{B29}$$

where

$$e_V S_{T,F} = \frac{\gamma_V}{6} I_V \Omega^2 \xi_V \left(-A_1 \cos\psi - B_1 \sin\psi - \bar{\beta} + \frac{q}{\Omega}\cos\psi + \frac{p}{\Omega}\sin\psi\right) \tag{B30}$$

$$e_V S_{I,F} = -\sigma_V \Omega^2 \bar{\bar{\beta}} e_V \tag{B31}$$

$$e_V S_{G,F} = 2e_V \Omega \bar{\tau}\left(\sigma_V + e_V \frac{W}{g}\right) \tag{B32}$$

$$e_V S_{AA,F} = e_V\left(\sigma_V + e_V \frac{W}{g}\right)(\dot{p}\sin\psi + \dot{q}\cos\psi) \tag{B33}$$

and

$$W = \int_{e_V}^{R} mg\, dr$$

Substituting for $\bar{\tau}$ in equation (B32) gives

$$e_V S_{G,F} = e_V\left(\sigma_V + e_V \frac{W}{g}\right)(2\Omega p\cos\psi - 2\Omega q\sin\psi) \tag{B34}$$

Therefore, the general equation for the total offset shear moment per blade is

$$e_V S_{VF} = \frac{\gamma_V}{6}\Omega^2 I_V \xi_V\left(-A_1\cos\psi - B_1\sin\psi - \bar{\beta}_1 + \frac{q}{\Omega}\cos\psi + \frac{p}{\Omega}\sin\psi\right) - 2\Omega q k_2 \sigma_V e_V \sin\psi$$

$$+ 2\Omega p k_2 \sigma_V e_V \cos\psi - \sigma_V \Omega^2 \bar{\bar{\beta}} e_V + k_2 \sigma_V e_V \dot{p}\sin\psi + k_2 \sigma_V e_V \dot{q}\cos\psi \tag{B35}$$

where

$$k_2 \approx 1 + 2\xi_v \tag{B36}$$

Separating $\sin\psi$ and $\cos\psi$ terms, dividing through by $I_v\Omega^2$, and combining with equations (B27), (B21), (B22), and (B23) for moments at the virtual flapping hinge give the following equations for longitudinal rotor-hub-moment increments:

$$\Delta\left(\frac{M_{H,A}}{I_v\Omega^2}\right)_{A_1} = \frac{n}{2}\left\{\frac{8C_1{}^2\Gamma_F}{k_3\gamma_v} + \frac{\gamma_v}{6}\xi_v\left(1 - \Gamma_F\right)\right\} \tag{B37}$$

$$\Delta\left(\frac{M_{H,A}}{I_v\Omega^2}\right)_{B_1} = -\frac{n}{2}\left\{C_1 + \frac{4}{3}\frac{C_1\xi_v}{k_3}\right\}\Gamma_F \tag{B38}$$

$$\Delta\left(\frac{M_{H,A}}{I_v\Omega}\right)_q = -\frac{n}{2}\left\{\frac{16C_1}{k_3\gamma_v}\left(K_{1F} + \frac{C_1}{2}\right)\Gamma_F + \frac{\gamma_v}{6}\xi_v\left[1 - \left(1 - \frac{128C_1K_{1F}}{\left(k_3\gamma_v\right)^2}\right)\Gamma_F\right]\right\} \tag{B39}$$

$$\Delta\left(\frac{M_{H,A}}{I_v\Omega}\right)_p = \frac{n}{2}\left\{C_1\left(1 - \frac{128C_1K_{1F}}{\left(k_3\gamma_v\right)^2}\right)\Gamma_F + \frac{3\xi_v}{k_3}\left[\frac{8}{9}\left(K_{1F} + \frac{C_1}{2}\right)\Gamma_F - k_1k_2k_3\right]\right\} \tag{B40}$$

$$\Delta\left(\frac{M_{H,A}}{I_v}\right)_{\dot{p}} = \frac{n}{2}\left\{\frac{8C_1K_{1F}}{k_3\gamma_v} + \frac{64C_1\xi_vK_{1F}}{6k_3{}^2\gamma_v}\right\}\Gamma_F \tag{B41}$$

$$\Delta\left(\frac{M_{H,A}}{I_v}\right) = -\frac{n}{2}\left\{\frac{64C_1{}^2K_{1F}}{\left(k_3\gamma_v\right)^2}\Gamma_F + \frac{3}{2}\frac{\xi_v}{k_3}\left(k_1k_2k_3 - \frac{8}{9}K_{1F}\Gamma_F\right)\right\} \tag{B42}$$

where

$$C_1 = K_{1F} - 1 + \left(\frac{\omega_{1NR}}{\Omega}\right)^2 \tag{B43}$$

and

$$k_1 = \frac{2}{3}\frac{\sigma_V R}{I_V} \tag{B44}$$

The following equalities exist between the lateral and longitudinal hub moments:

$$\left.\begin{aligned}
\Delta\left(\frac{M_{H,B}}{I_V\Omega^2}\right)_{A_1} &= -\Delta\left(\frac{M_{H,A}}{I_V\Omega^2}\right)_{B_1} \\
\Delta\left(\frac{M_{H,B}}{I_V\Omega^2}\right)_{B_1} &= \Delta\left(\frac{M_{H,A}}{I_V\Omega^2}\right)_{A_1} \\
\Delta\left(\frac{M_{H,B}}{I_V\Omega}\right)_{q} &= -\Delta\left(\frac{M_{H,A}}{I_V\Omega}\right)_{p} \\
\Delta\left(\frac{M_{H,B}}{I_V\Omega}\right)_{p} &= \Delta\left(\frac{M_{H,A}}{I_V\Omega}\right)_{q} \\
\Delta\left(\frac{M_{H,B}}{I_V}\right)_{\dot{q}} &= -\Delta\left(\frac{M_{H,A}}{I_V}\right)_{\dot{p}} \\
\Delta\left(\frac{M_{H,B}}{I_V}\right)_{\dot{p}} &= \Delta\left(\frac{M_{H,A}}{I_V}\right)_{\dot{q}}
\end{aligned}\right\} \tag{B45}$$

APPENDIX C

DERIVATION OF ONCE-PER-ROTOR-REVOLUTION CHORDWISE STRUCTURAL BENDING-MOMENT EQUATION USING EQUIVALENT HINGED BLADE ANALYSIS

The equivalent uniform blade hinge offset ξ_V in the chordwise (or lagging) degree of freedom is the same as in the flapping degree of freedom and the spring restraint about the virtual lagging hinge K_{VL} is given by equation (9). The summation of moments about the virtual lagging hinge is

$$\sum M_{VL} = M_{T,L} + M_{C,L} + M_{CF,L} + M_{I,L} + M_{S,L} = 0 \tag{C1}$$

The expression for blade lagging moment due to Coriolis forces is

$$M_{C,L} = -2I_V\Omega^2 a_o\bar{\beta}_1 \tag{C2}$$

The expression for blade lagging moment due to centrifugal force is

$$M_{CF,L} = -\sigma_V e_V \Omega^2 \zeta_1 \tag{C3}$$

The expression for blade lagging moment due to inertia force is

$$M_{I,L} = -I_V\Omega^2\ddot{\bar{\zeta}}_1 \tag{C4}$$

The expression for blade lagging moment due to the virtual lagging hinge spring is

$$M_{S,L} = -K_{VL}\zeta_1 \tag{C5}$$

If the aerodynamic drag moment contribution is neglected, the expression for the aerodynamic lagging moment in hover flight is (fig. 4)

$$M_{T,L} \approx -\int_{e_V}^{BR} \frac{1}{2}\rho U^2 c r c_l \sin\phi \, dr \tag{C6}$$

or for small angles

$$M_{T,L} = -\int_{e_V}^{BR} \frac{1}{2}\rho U^2 c r a \alpha\phi \, dr$$

APPENDIX C

The first harmonic terms in the product $\alpha\phi$ are retained from the multiplication of equations (B13) and (B16) as follows:

$$(\alpha\phi)_{\sin\psi} = -\frac{2\lambda_s}{x}a_1 + \frac{2\lambda_s}{x}\frac{p}{\Omega} - \frac{\lambda_s}{x}B_1 - \theta_o a_1 - \theta_t x a_1 + \theta_o\frac{p}{\Omega} + \theta_t x\frac{p}{\Omega} \tag{C7}$$

$$(\alpha\phi)_{\cos\psi} = \frac{2\lambda_s}{x}b_1 + \frac{2\lambda_s}{x}\frac{q}{\Omega} - \frac{\lambda_s}{x}A_1 + \theta_o b_1 + \theta_t x b_1 + \theta_o\frac{q}{\Omega} + \theta_t x\frac{q}{\Omega} \tag{C8}$$

where

$$\lambda_s = -\frac{v}{\Omega R} \qquad \text{(For hover)} \tag{C9}$$

Given

$$\tau \equiv -q\cos\psi - p\sin\psi \tag{C10}$$

Substituting equations (C7), (C8), and (C10) into equation (C6) along with equations (B18), (B21), and (B10) and combining terms gives

$$M_{T,L} = -\gamma_v I_v \Omega^2\left[\left(-\frac{1}{3}\lambda_s - \frac{1}{8}\theta_o - \frac{1}{10}\theta_t\right)\bar{\beta}_1 + \left(-\frac{1}{3}\lambda_s - \frac{1}{8}\theta_o - \frac{1}{10}\theta_t\right)\tau + \left(\frac{1}{6}\lambda_s\right)\theta_1\right] \tag{C11}$$

The general lagging equation of motion becomes

$$\ddot{\zeta}_1 + \left(\frac{K_{VL}}{I_v\Omega^2} + \frac{\sigma_v e_v}{I_v}\right)\zeta_1 + \gamma_v\left[\left(-\frac{\lambda_s}{3} - \frac{\theta_o}{8} - \frac{\theta_t}{10}\right)\left(\bar{\beta}_1 + \frac{\tau}{\Omega}\right) + \frac{\lambda_s}{6}\theta_1\right] + 2a_o\bar{\beta}_1 = 0 \tag{C12}$$

Assuming first-harmonic sinusoidal motion gives the following general expression for lagging motion:

$$\zeta_1 = \Gamma_L\left[\gamma_v\left(\frac{\lambda_s}{3} + \frac{\theta_o}{8} + \frac{\theta_t}{10}\right)\left(\bar{\beta} - \frac{\tau}{\Omega}\right) - \gamma_v\frac{\lambda_s}{6}\theta_1 - 2a_o\bar{\beta}_1\right] \tag{C13}$$

where

$$\Gamma_L = \left[\left(\frac{\nu_{1NR}}{\Omega}\right)^2 + \frac{3}{2}k_1\xi_v - 1\right]^{-1} \tag{C14}$$

If the flapping hinge spring restraint is neglected, which is generally small compared to centrifugal stiffening at operating rotor speed, is neglected,

$$a_o \approx \gamma_v\left(\frac{\lambda_s}{6} + \frac{\theta_o}{8} + \frac{\theta_t}{10} - \frac{M_W\eta}{\gamma_v I_v \Omega^2}\right) \tag{C15}$$

Substituting equation (C15) into equation (C13) gives

$$\zeta_1 = \Gamma_L\gamma_v\left[-\left(\frac{\theta_o}{8} + \frac{\theta_t}{10} - \frac{2M_W\eta}{\gamma_v I_v \Omega^2}\right)\bar{\beta} - \left(\frac{\lambda_s}{6}\right)\theta_1 + \frac{1}{\Omega}\left(\frac{\lambda_s}{3} + \frac{\theta_o}{8} + \frac{\theta_t}{10}\right)\tau\right] \tag{C16}$$

The structural moment transmitted across the virtual lagging hinge is

$$M_{VL} = K_{VL}\zeta_1 \tag{C17}$$

Therefore

$$M_{VL} = K_{VL}\Gamma_L\gamma_v\left[-\left(\frac{\theta_o}{8} + \frac{\theta_t}{10} - \frac{2M_W\eta}{\gamma_v I_v \Omega^2}\right)\bar{\beta} - \left(\frac{\lambda_s}{6}\right)\theta_1 + \frac{1}{\Omega}\left(\frac{\lambda_s}{3} + \frac{\theta_o}{8} + \frac{\theta_t}{10}\right)\tau\right] \tag{C18}$$

Equation (C18) represents the superposition of the force inputs in the lagging degree of freedom due to $\bar{\beta}_1$, θ_1, and τ which are seen as functions of ψ by the rotating blade as follows:

$$\left.\begin{aligned} \bar{\beta}_1 &= |\beta_1|\cos\left(\psi - \psi_{\beta,1} + \frac{\pi}{2}\right) \\ \theta_1 &= |\theta_1|\cos\left(\psi - \psi_{\theta,1}\right) \\ \tau &= |\tau|\cos\left(\psi - \psi_\tau\right) \end{aligned}\right\} \tag{C19}$$

Therefore, equation (C18) can be written as a function of azimuth angle as follows:

$$M_{VL}(\psi) = K_{VL}\Gamma_L\gamma_v\left[C_2|\beta_1|\cos\left(\psi - \psi_{\beta,1} + \frac{\pi}{2}\right) + C_3|\tau|\cos\left(\psi - \psi_\tau\right) + C_4|\theta_1|\cos\left(\psi - \psi_{\theta,1}\right)\right] \tag{C20}$$

where

$$\psi = \Omega t$$

and

$$C_2 = -\left(\frac{\theta_o}{8} + \frac{\theta_t}{10} - \frac{2M_W\eta}{\gamma_V I_V \Omega^2}\right) \tag{C21}$$

$$C_3 = \frac{1}{\Omega}\left(\frac{\theta_o}{8} + \frac{\theta_t}{10} + \frac{\lambda_s}{3}\right) \tag{C22}$$

$$C_4 = -\frac{\lambda_s}{6} = \frac{1}{6}\left(\frac{C_T}{2}\right)^{1/2} \tag{C23}$$

During a hovering maneuver the following terms in equation (C20) are functions of time t:

$$\left.\begin{aligned}
&|\beta_1| = |\beta_1(t)| = \left[a_1(t)^2 + b_1(t)^2\right]^{1/2} \\
&|\tau| = |\tau(t)| = \left[q(t)^2 + p(t)^2\right]^{1/2} \\
&|\theta_1| = |\theta_1(t)| = \left[A_1(t)^2 + B_1(t)^2\right]^{1/2} \\
&\psi_{\beta,1} = \psi_{\beta,1}(t) = \tan^{-1}\frac{-b_1(t)}{-a_1(t)} \\
&\psi_\tau = \psi_\tau(t) = \tan^{-1}\frac{-p(t)}{-q(t)} \\
&\psi_{\theta,1} = \psi_{\theta,1}(t) = \tan\frac{-B_1(t)}{-A_1(t)}
\end{aligned}\right\} \tag{C24}$$

The aircraft normal load factor η in equation (C20) is also a function of time t during the maneuver.

REFERENCES

1. Gustafson, F. B.: Powered-Lift Research at Langley Field. J. Roy. Aeron. Soc., vol. 67, no. 630, June 1963, pp. 371-377.

2. Cresap, W. L: Rigid Rotor Development and Flight Tests. J. Am. Helicopter Soc., vol. 7, no. 2, Apr. 1962, pp. 32-41.

3. Statler, W. H.; Heppe, R. R.; and Cruz, E. S.: Results of the XH-51A Rigid Rotor Research Helicopter Program. Proc. Nineteenth Ann. Nat. Forum, Am. Helicopter Soc., May 1963, pp. 119-133.

4. Huston, Robert J.: An Exploratory Investigation of Factors Affecting the Handling Qualities of a Rudimentary Hingeless Rotor Helicopter. NASA TN D-3418, 1966.

5. Young, Maurice I.: A Simplified Theory of Hingeless Rotors With Application to Tandem Helicopters. Proc. Eighteenth Ann. Natl. Forum, Am. Helicopter Soc., Inc., May 1962, pp. 38-45.

6. Yntema, Robert T.: Simplified Procedures and Charts for the Rapid Estimation of Bending Frequencies of Rotating Beams. NACA TN 3459, 1955. (Supersedes NACA RM L54G02.)

7. Brooks, George W.: On the Determination of the Chordwise Bending Frequencies of Rotor Blades. J. Am. Helicopter Soc., vol. 3, no. 3, July 1958, pp. 40-42.

8. Gessow, Alfred; and Crim, Almer D.: A Method for Studying the Transient Blade-Flapping Behavior of Lifting Rotors at Extreme Operating Conditions. NACA TN 3366, 1955.

9. McCloud, John L., III; and Biggers, James C.: Full-Scale Wind-Tunnel Tests of a Nonarticulated Helicopter Rotor. NASA TN D-2392, 1964.

10. Ward, John F.; and Huston, Robert J.: A Summary of Hingeless-Rotor Research at NASA – Langley. Proc. Twentieth Ann. Natl. Forum, Am. Helicopter Soc., Inc., May 1964, pp. 76-83.

11. Lockheed-California Co.: Investigation of Elastic Coupling Phenomena of High Speed Rigid Rotor Systems. TRECOM Tech. Rept. 63-75 (Lockheed Rept. No. 17013), U.S. Army Transportation Res. Command (Fort Eustis, Va.), June 1964.

12. Huston, Robert J.; and Ward, John F.: Handling Qualities and Structural Characteristics of the Hingeless-Rotor Helicopter. Conference on V/STOL and STOL Aircraft, NASA SP-116, 1966, pp. 1-16.

"The aeronautical and space activities of the United States shall be conducted so as to contribute . . . to the expansion of human knowledge of phenomena in the atmosphere and space. The Administration shall provide for the widest practicable and appropriate dissemination of information concerning its activities and the results thereof."

—NATIONAL AERONAUTICS AND SPACE ACT OF 1958

NASA SCIENTIFIC AND TECHNICAL PUBLICATIONS

TECHNICAL REPORTS: Scientific and technical information considered important, complete, and a lasting contribution to existing knowledge.

TECHNICAL NOTES: Information less broad in scope but nevertheless of importance as a contribution to existing knowledge.

TECHNICAL MEMORANDUMS: Information receiving limited distribution because of preliminary data, security classification, or other reasons.

CONTRACTOR REPORTS: Technical information generated in connection with a NASA contract or grant and released under NASA auspices.

TECHNICAL TRANSLATIONS: Information published in a foreign language considered to merit NASA distribution in English.

TECHNICAL REPRINTS: Information derived from NASA activities and initially published in the form of journal articles.

SPECIAL PUBLICATIONS: Information derived from or of value to NASA activities but not necessarily reporting the results of individual NASA-programmed scientific efforts. Publications include conference proceedings, monographs, data compilations, handbooks, sourcebooks, and special bibliographies.

Details on the availability of these publications may be obtained from:

SCIENTIFIC AND TECHNICAL INFORMATION DIVISION

NATIONAL AERONAUTICS AND SPACE ADMINISTRATION

Washington, D.C. 20546